



OPEN ACCESS

EDITED BY

Bin Gong,
University of Texas Medical Branch at
Galveston, United States

REVIEWED BY

Chunlong Mu,
University of Calgary, Canada
Leonardo Santana Novaes,
Max Planck Institute for Biological
Cybernetics, Germany

*CORRESPONDENCE

Wai-Yin Cheng

✉ wai-yin-nano.cheng@polyu.edu.hk

Raymond Chuen-Chung Chang

✉ rccchang@hku.hk

RECEIVED 24 July 2024

ACCEPTED 06 February 2025

PUBLISHED 25 February 2025

CITATION

Cheng W-Y, Lee X-Z, Lai MS-L, Ho Y-S and
Chang RC-C (2025) PKR modulates sterile
systemic inflammation-triggered
neuroinflammation and brain glucose
metabolism disturbances.
Front. Immunol. 16:1469737.
doi: 10.3389/fimmu.2025.1469737

COPYRIGHT

© 2025 Cheng, Lee, Lai, Ho and Chang. This is
an open-access article distributed under the
terms of the [Creative Commons Attribution
License \(CC BY\)](#). The use, distribution or
reproduction in other forums is permitted,
provided the original author(s) and the
copyright owner(s) are credited and that the
original publication in this journal is cited, in
accordance with accepted academic
practice. No use, distribution or reproduction
is permitted which does not comply with
these terms.

PKR modulates sterile systemic inflammation-triggered neuroinflammation and brain glucose metabolism disturbances

Wai-Yin Cheng^{1,2,3*}, Xin-Zin Lee¹, Michael Siu-Lun Lai¹,
Yuen-Shan Ho⁴ and Raymond Chuen-Chung Chang^{1,5*}

¹Laboratory of Neurodegenerative Diseases, School of Biomedical Sciences, LKS Faculty of Medicine, The University of Hong Kong, Hong Kong, Hong Kong SAR, China, ²Research Institute for Future Food, The Hong Kong Polytechnic University, Hong Kong, Hong Kong SAR, China, ³Department of Food Science and Nutrition, Faculty of Science, The Hong Kong Polytechnic University, Hong Kong, Hong Kong SAR, China, ⁴School of Nursing, Faculty of Health and Social Sciences, Hong Kong Polytechnic University, Hong Kong, Hong Kong SAR, China, ⁵State Key Laboratory of Brain and Cognitive Sciences, The University of Hong Kong, Hong Kong, Hong Kong SAR, China

Sterile systemic inflammation may contribute to neuroinflammation and accelerate the progression of neurodegenerative diseases. The double-stranded RNA-dependent protein kinase (PKR) is a key signaling molecule that regulates immune responses by regulating macrophage activation, various inflammatory pathways, and inflammasome formation. This study aims to study the role of PKR in regulating sterile systemic inflammation-triggered neuroinflammation and cognitive dysfunctions. Here, the laparotomy mouse model was used to study neuroimmune responses triggered by sterile systemic inflammation. Our study revealed that genetic deletion of PKR in mice potently attenuated the laparotomy-induced peripheral and neural inflammation and cognitive deficits. Furthermore, intracerebroventricular injection of rAAV-DIO-PKR-K296R to inhibit PKR in cholinergic neurons of ChAT-IRES-Cre-eGFP mice rescued the laparotomy-induced changes in key metabolites of brain glucose metabolism, particularly the changes in phosphoenolpyruvate and succinate levels, and cognitive impairment in short-term and spatial working memory. Our results demonstrated the critical role of PKR in regulating neuroinflammation, brain glucose metabolism and cognitive dysfunctions in a peripheral inflammation model. PKR could be a novel pharmacological target for treating systemic inflammation-induced neuroinflammation and cognitive dysfunctions.

KEYWORDS

laparotomy, microglia, neuroimmune responses, peripheral inflammation, postoperative cognitive dysfunction, protein kinase R, targeted metabolomics

1 Introduction

Systemic inflammation may promote neuroinflammation and neurodegeneration (1–3). Neuroinflammation contributes to neurodegenerative disorders, including Alzheimer's disease (AD) (4), Parkinson's disease (PD) (5), and amyotrophic lateral sclerosis (6). During systemic inflammation, the infiltration of circulating cytokines and macrophages into the brain can activate microglia (7, 8). Activated microglia release pro-inflammatory cytokines, leading to neuronal injury and death (9). These inflammatory mediators can further facilitate the recruitment of leukocyte into the brain, perpetuating neuroinflammation (10).

This study utilizes a nonbacterial endotoxin mouse model of laparotomy to address the sterile systemic inflammation triggered by surgery. This laparotomy model is suitable for investigating perioperative neurocognitive disorder (PND) (11). As a surgical model, laparotomy (12, 13) outperforms other experimental models including tibial fracture surgery (14–16) for studying peripheral inflammation because it allows for a longer period of observation up to 2 weeks. Unlike non-sterile models involving injection of bacteria (17) or lipopolysaccharide (LPS) (18, 19), the laparotomy model induces a sterile inflammatory response, more closely mimicking the conditions of many surgical procedures. Therefore, the laparotomy model is appropriate for the investigation of whether and how neuroinflammation leads to cognitive dysfunctions upon sterile systemic inflammation.

In this study, we focused on the liver, frontal cortex, and hippocampus, as these regions are critically involved in systemic inflammation-induced neuroinflammation and cognitive deficits. The liver, a critical immunological organ, is the largest reservoir of tissue-resident macrophages—Kupffer cells—which account for 80% of all macrophages in the body (20). Constantly exposed to antigen- and cytokine-rich blood from the gut and systemic circulation, the liver plays a critical role in innate immune responses and is highly sensitive to peripheral inflammation. Our focus on the liver aligns with our interest in monocytes/macrophages rather than T/B cells. Therefore, we specifically focused on the liver in this sterile systemic inflammation mouse model, rather than examining other immune organs such as the spleen or lymph nodes. The frontal cortex and hippocampus were selected because they are essential for memory, learning, and executive function, processes known to be impaired in systemic inflammation-induced neuroinflammation. These brain regions are highly vulnerable to inflammation-induced damage, making them ideal targets for investigating the roles of PKR in neuroinflammation and cognitive deficits. While other regions, such as the basal forebrain, are relevant to the roles of PKR in cholinergic signaling, they were outside the scope of this study and will be examined in future investigations.

Double-stranded RNA-dependent protein kinase (PKR), which is a serine/threonine kinase encoded in humans by the EIF2AK2 gene, regulates mRNA translation, transcription, proliferation, and apoptosis (21). In addition to its established antiviral role, PKR is a key signaling molecule that modulates immune responses by regulating the activation of macrophages (22), various inflammatory pathways, and formation of inflammasomes (23). PKR can be activated by various stimuli, including cytokines, double-stranded RNA (dsRNA) produced

by virus, bacterial LPS, and growth factors (23). Activation of PKR could regulate the activation of various critical inflammatory kinases, including mitogen-activated protein kinases (MAPKs) (24) and inhibitor of nuclear factor- κ B (I κ B) kinase (25). Furthermore, PKR activates and regulates the release of inflammasome-dependent cytokines (26, 27). Therefore, PKR is critical in regulating inflammatory responses.

In addition to regulating immune responses, PKR plays an essential role in cognition and age-related neurodegeneration. Our laboratory was among the first to reveal that PKR activation and eukaryotic initiation factor-2alpha (eIF2 α) phosphorylation are implicated in neuronal apoptosis (28). The overexpression of wild-type PKR in human neuroblastoma cells could enhance the apoptosis induced by β -amyloid peptides; while overexpression of dominant-negative PKR could attenuate the induced apoptosis. Primary cultured neurons from PKR knockout mice showed greater tolerance to β -amyloid neurotoxicity compared with their wild-type counterpart (28). In addition, knockout of PKR could result in the enhanced late-phase long-term potentiation (LTP) in hippocampal sections, increased network excitability, as well as improved cognitive functions with the enhancement of learning and memory in mice (29). Recently, PKR has also been linked to glucose metabolism regulation (30, 31). Metabolic reprogramming, a process by which cells alter their energy production and utilization pathways in response to stress or pathological conditions, is crucial in inflammation and neurodegeneration (32, 33). Brain glucose hypometabolism, characterized by reduced glucose utilization, is a hallmark of neurodegenerative diseases including AD and PD in their preclinical stages (34, 35). The involvement of PKR in both neuronal function and metabolic processes suggests a potential mechanistic link between these pathways. Collectively, these studies suggest the role of PKR in modulating cognitive functions, neurodegeneration, and potentially, metabolic processes in the brain. Given that global knockout of PKR in mice affects glucose metabolism (30, 36, 37), which would confound the interpretation of brain-specific effects, we focused on studying whether inhibition of PKR in cholinergic neurons affects brain glucose metabolism in the laparotomy model.

Cholinergic neurons, particularly those in the basal forebrain, play a crucial role in regulating cognitive functions and are known to be involved in regulating glucose metabolism (38, 39). These neurons are particularly vulnerable to degeneration in conditions like Alzheimer's disease (AD), emphasizing the need to understand factors that affect their function. Given that PKR is involved in metabolic regulation, investigating the roles of PKR in cholinergic neurons could uncover mechanisms by which these neurons influence brain glucose metabolism.

Considering the established roles of PKR in modulating immune responses, cognition and glucose metabolism, we hypothesize that PKR regulates the progression of inflammation from the periphery to the brain, and PKR in cholinergic neurons can modulate cognitive functions, potentially associated with modulating brain glucose metabolism. This project aims at investigating whether PKR can be a novel pharmacological target for preventing systemic inflammation-triggered neuroinflammation and cognitive deficits.

2 Materials and methods

2.1 Animal husbandry

Male wild-type C57BL/6J, C57BL/6-Tg(CD68-EGFP)1Drg/J (referred to herein as CD68-eGFP mice), PKR^{-/-}, and ChAT-IRES-Cre-eGFP mice (3 months) were obtained from the Centre for Comparative Medicine Research of the University of Hong Kong. This center is fully accredited by the Association for Assessment and Accreditation of Laboratory Animal Care. The mice were housed in cages under controlled temperature (20°C – 22°C), humidity (50% – 60%), with a 12 hour light/dark cycle and ad libitum access to food and water. Mice were allowed to acclimate for 1 week prior to experiment. Only male mice were used to avoid the potential confounding effects of hormonal fluctuations during the female estrous cycle, which could interfere with the interpretation of the role of the PKR in modulating systemic inflammation-triggered neuroinflammation and cognitive dysfunction that we aimed to investigate.

2.2 Experimental protocols

Laparotomy was used as a model to examine neuroimmune responses induced by systemic inflammation. The experimental

workflow is summarized in Figure 1. In part 1, male wild-type C57BL/6J and CD68-eGFP mice were randomized into two groups: laparotomy with sevoflurane anesthesia and control group with sevoflurane anesthesia alone. In part 2, the PKR^{-/-} mice were exposed to laparotomy with sevoflurane anesthesia or sevoflurane anesthesia only to examine the role of PKR in regulating systemic inflammation-triggered neuroinflammation and cognitive deficits. In part 3, rAAV-DIO-PKR-K296R was intracerebroventricularly injected into the right lateral ventricle of ChAT-IRES-Cre-eGFP mice to suppress PKR activation specifically in cholinergic neurons. Mice were then subjected to laparotomy with sevoflurane or sevoflurane anesthesia alone. This allowed examination of the regulatory effects of blocking PKR in cholinergic neurons on glucose metabolism and cognitive function in the laparotomy model.

2.3 Laparotomy

For anesthetization, the animal was placed in a chamber with 5% sevoflurane (Sevorane™, Abbott, Switzerland) and transferred to a nose mask with anesthesia maintained at 3% sevoflurane with a gas flow of 800 ml/min using an inhalation anesthesia machine (Harvard, US). The laparotomy procedure followed previous descriptions with modifications (12). Hair was removed from the surgical site, and the skin was disinfected. A 2 cm longitudinal midline cut was made at 0.5

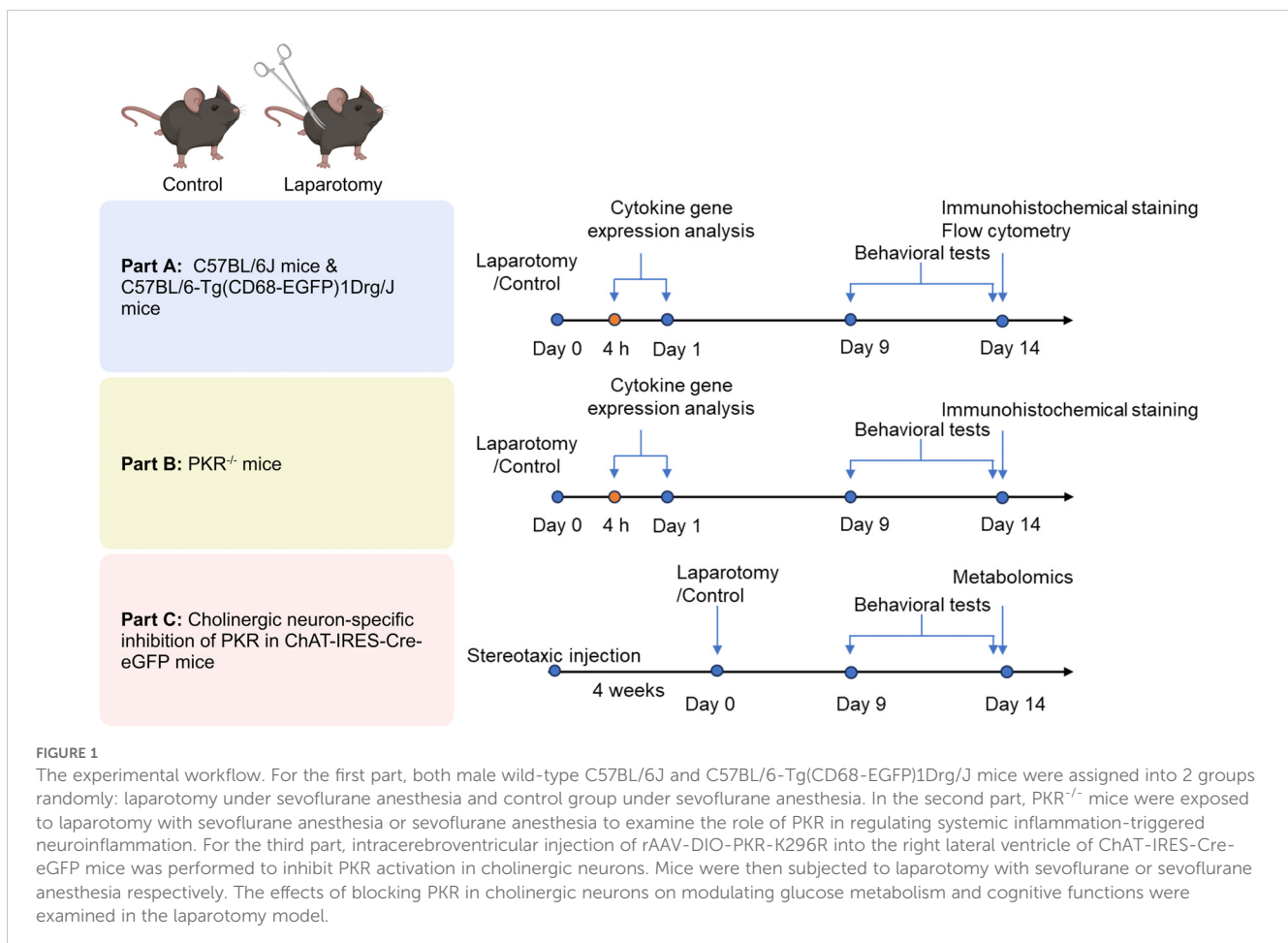


FIGURE 1

The experimental workflow. For the first part, both male wild-type C57BL/6J and C57BL/6-Tg(CD68-EGFP)1Drg/J mice were assigned into 2 groups randomly: laparotomy under sevoflurane anesthesia and control group under sevoflurane anesthesia. In the second part, PKR^{-/-} mice were exposed to laparotomy with sevoflurane anesthesia or sevoflurane anesthesia to examine the role of PKR in regulating systemic inflammation-triggered neuroinflammation. For the third part, intracerebroventricular injection of rAAV-DIO-PKR-K296R into the right lateral ventricle of ChAT-IRES-Cre-eGFP mice was performed to inhibit PKR activation in cholinergic neurons. Mice were then subjected to laparotomy with sevoflurane or sevoflurane anesthesia respectively. The effects of blocking PKR in cholinergic neurons on modulating glucose metabolism and cognitive functions were examined in the laparotomy model.

cm below the lower right rib. A small intestinal segment of approximately 10 cm length was temporarily exteriorized and subjected to 2 minutes of gentle manipulation before being replaced in the abdomen. Abdominal muscle and skin suture was conducted using 5-0 vicryl and nylon suture respectively (Ethicon, USA).

2.4 Stereotaxic injection

Mice were anesthetized by intraperitoneal injection of a ketamine/xylazine mixture (80 mg/kg and 8 mg/kg, respectively). Prior to surgery, hair was removed from the surgical site, and the skin was disinfected. The head was then fixed onto a stereotaxic frame (Narishige, Japan). A 1.5 cm straight midline incision was made to expose the skull. Either rAAV-DIO-PKR-K296R (packaged in AAV serotype 6) (2 μ l; 1×10^{13} vg/mL) or 0.9% saline was injected intracerebroventricularly into right lateral ventricle (antero-posterior: -0.6 mm, medial-lateral: -1.3 mm, dorsal-ventral: -3.1 mm) at a flow rate of 0.5 μ L/min using a Hamilton syringe, 33-gauge needle (7803-05, Hamilton, USA). Following the injection, the needle was retained *in situ* for 5 min allowing the solution to diffuse and avoiding solution backflow. The incision site was sealed with a nonabsorbable nylon suture (5-0, PS-2; Ethicon, USA). At 4 weeks following stereotaxic injection, mice were randomized into different groups subjected to either laparotomy with sevoflurane or sevoflurane anesthesia respectively.

2.5 Open field test

Open field test (OFT) is adopted to assess locomotor activity, exploratory behavior and anxiety in mice based on their innate propensity to avoid open spaces (40). Mice were placed in a 40 cm square arena and allowed to freely explore for 10 min. Total distance traveled and time spent exploring central area were quantified as indices of locomotor activity and anxiety.

2.6 Novel object recognition test

Novel object recognition test (NOR) assesses recognition memory in mice based on their innate preference for novelty (41). In the training session, mice were first allowed to explore an open field arena with two identical objects (A + A) for 10 min. After 24 hours, mice were allowed to explore the familiar arena with a novel object replacing one of the identical objects (A + B). Basically, driven by curiosity, the mice would spend more time exploring the novel object rather than the familiar one. The discrimination index, calculated as a ratio of time exploring the novel versus familiar object, can be regarded as an index of recognition memory.

2.7 Spontaneous alternation Y-maze test

Spontaneous alternation Y-maze (SYM) test assesses short-term spatial working memory in rodents. Mice are allowed to explore the

maze for 5 min (42). A spontaneous alternation involves three successive entries into a new arm rather than returning to an earlier one. Driven by curiosity, the mice will tend to explore the new arm rather than the previously visited arm. The percentage of alternation was determined by dividing the number of spontaneous alternations by the total arm entries, then multiplying by 100. The percentage of alternation can be the indicator of short-term spatial working memory.

2.8 Puzzle box test

A puzzle box test was a five-day protocol modified by our laboratory (41) based on the previous published method (43). It is designed to assess rodent's native problem-solving ability, short-term and long-term memory. The puzzle box consisted of two main sections: an open-field area (600 \times 280 mm) and an adjacent sheltered goal-box area (150 \times 280 mm). Mice could enter the sheltered goal-box arena through a small underpass between these two compartments. Mice were required to complete escape tasks of increasing difficulty within a fixed period of time (Supplementary Table S1). The first four days involved three trials per day, while the final day comprised a single trial. Each obstruction includes three trials; the initial two taking place on the same day, with the third trial conducted on the following day. Three trials were performed: the first evaluated problem-solving skills; the second assessed short-term memory, and the third investigated long-term memory.

2.9 Arrangement of behavioral tests

A series of cognitive behavioral tests was conducted based on the following schedule. For minimized fatigue and interference, behavioral tests were divided across the study. A group of mice underwent OFT on postoperative day (POD) 10, followed by NOR on POD 11–12. A second group of mice underwent OFT on POD 10, followed by SYM on POD 11. The third cohort completed OFT on POD 9 and the puzzle box test on POD 10–14.

2.10 RNA extraction and quantitative real-time RT-PCR

Mice were euthanized by carbon dioxide asphyxiation and decapitation, in line with the protocols recommended by American Veterinary Medical Association and then followed by transcardial perfusion with ice-cold saline. Frontal cortex, hippocampus, and liver were harvested, snap-frozen, and kept at -80°C . Total RNA was isolated from samples using the RNAiso Plus (TAKARA, Japan). Detailed protocols were described in Supplementary Methods. Quantitative real-time RT-PCR was performed with TB Green[®] Premix Ex Taq[™] II (TAKARA, Japan) using a Bio-Rad CFX 96 real-time PCR detection system (Bio-Rad, USA) in triplicate. Primer sequences utilized for amplification are provided in Supplementary Table S2. Relative expression was determined using the comparative CT method, normalizing the target gene mRNA to GAPDH.

2.11 Immunohistochemical staining and confocal microscopy

Following euthanasia by CO₂ asphyxiation, mice were perfused transcardially with ice-cold saline. The brains were then removed and post-fixed in 4% paraformaldehyde for 24 h at 4°C. The processes for cryosection preparation described in the [Supplementary Methods](#) were similar to those described previously for human brain sections (28). Prior to confocal imaging, brain slices were pretreated with 10% goat serum blocking solution, followed by overnight incubation at 4°C with primary antibodies listed in [Supplementary Table S3](#), followed by 1h secondary antibody staining (Alexa Fluor, 1:400, Invitrogen) at room temperature and co-staining with 4', 6-diamidino-2-phenylindole (DAPI). Confocal images were acquired using a LSM800 confocal microscope (Carl Zeiss, Germany) with 10× or 20× objective or 40× oil immersion objective using Zen Blue software. The frame size was set to 1024 × 1024 pixels, the bit depths to 16-bit, averaging to 2×, and pinhole setting at 1 airy unit. Z-stack images were acquired, followed by orthogonal projections from Z-stack images using Zen Blue software. Image analysis was performed using ImageJ software (National Institute of Health, USA).

2.12 Flow cytometry

The frontal cortex and hippocampus of CD68-eGFP mice were collected, processed through homogenization and filtration to obtain single-cell suspensions, which were then stained with DAPI. Detailed protocol was described in the [Supplementary Methods](#). Cellular fluorescence was measured using an Agilent NovoCyte Quanteon analyzer (Agilent, USA).

2.13 Targeted metabolomics by GC-MS/MS

Samples were obtained from the collected frontal cortex on POD 14 and prepared using the protocol described in the [Supplementary Methods](#). Targeted metabolomics of polar compounds in central carbon metabolism was performed using gas chromatography-tandem mass spectrometry (GC-MS/MS) on Agilent 7890B GC-Agilent 7010 Triple Quadrupole Mass Spectrometer system (Agilent, USA). The experimental parameters were stated in the [Supplementary Methods](#). Data were normalized by median and log-transformed. Heat map and hierarchical clustering were conducted based on Euclidian distance using Ward's algorithm. Further principal component analysis (PCA) and partial least squares discriminant analysis (PLS-DA) were further performed using Metaboanalyst 5.0.

2.14 Statistical analysis

Unless otherwise specified, all statistical analyses were performed on Prism v8.0c (GraphPad Software, USA). Data were expressed as means ± SEM. The normality of data were assessed

using the D'Agostino-Pearson normality test. Unpaired two-tailed Student's t-test at $p < 0.05$ was applied for comparing two group to determine the statistical significance of treatment effects. Interactions between mouse strain and treatment were assessed using two-way ANOVA with Bonferroni *post hoc* test. Statistical significance was set at $p < 0.05$.

3 Results

3.1 Laparotomy induced peripheral and neural inflammation in wild-type mice

To investigate the systemic and neural immune responses following the laparotomy challenge, we initially performed laparotomy in the C57BL/6J mice. Four hours following surgery, *interleukin (IL)-1 β* and *monocyte chemoattractant protein (MCP)-1* mRNA expression were enhanced in the liver of the laparotomy group when compared with that in the control counterpart ($p < 0.05$; [Figure 2A](#)). *IL-1 β* expression was also significantly upregulated in the hippocampus following the laparotomy challenge ($p < 0.05$; [Figure 2A](#)). On POD 1, no significant differences in *IL-1 β* , *IL-6*, *MCP-1*, and *tumour necrosis factor-alpha (TNF- α)* mRNA expression in the liver were found between the laparotomy and control groups ([Figure 2B](#)). This finding implied that the induced systemic inflammation is relatively transient. However, laparotomy significantly increased *IL-1 β* and *IL-6* expression in the frontal cortex and hippocampus versus controls ($p < 0.05$; [Figure 2B](#)), indicating ongoing, persistent neuroimmune responses.

To further study the effects of laparotomy on neuroinflammation, we utilized transgenic CD68-eGFP mice for visualizing microglia/macrophage dynamics. The CD68-eGFP mice expressed high levels of enhanced green fluorescent protein (eGFP) in macrophages and activated microglia, which aided in identifying activated microglia and macrophages. Brain sections were immunostained with antibodies against eGFP, TMEM119 (transmembrane protein 119: a microglia-specific marker), and CD105 (endoglin: a vascular endothelial marker). On POD 14, more CD68-eGFP-positive cells were observed in the frontal cortex ($p < 0.01$) and hippocampus (including cornu ammonis (CA)1 and CA3 ($p < 0.05$), as well as dentate gyrus (DG) ($p < 0.01$)) of the laparotomy mice compared with those of the control counterpart ([Supplementary Figures S1, S2](#)). Furthermore, an increased number of vessel-associated macrophages (CD68-eGFP⁺, TMEM119⁻ cells associated with the blood vessels) in the frontal cortex was detected following laparotomy ($p < 0.05$; [Supplementary Figures S1A, B](#)). This result suggested the activation of microglia/potential infiltration of macrophages following laparotomy. Flow cytometry also demonstrated elevated numbers of CD68-eGFP-positive cells in both frontal cortex and hippocampus on POD 14 when compared to controls ($p < 0.05$; [Figures 2C-F](#)), suggesting laparotomy induced the activation of microglia/potential infiltration of macrophages in the brain.

Brain sections from the CD68-eGFP mice were immunostained with a microglial marker, ionized calcium-binding adaptor

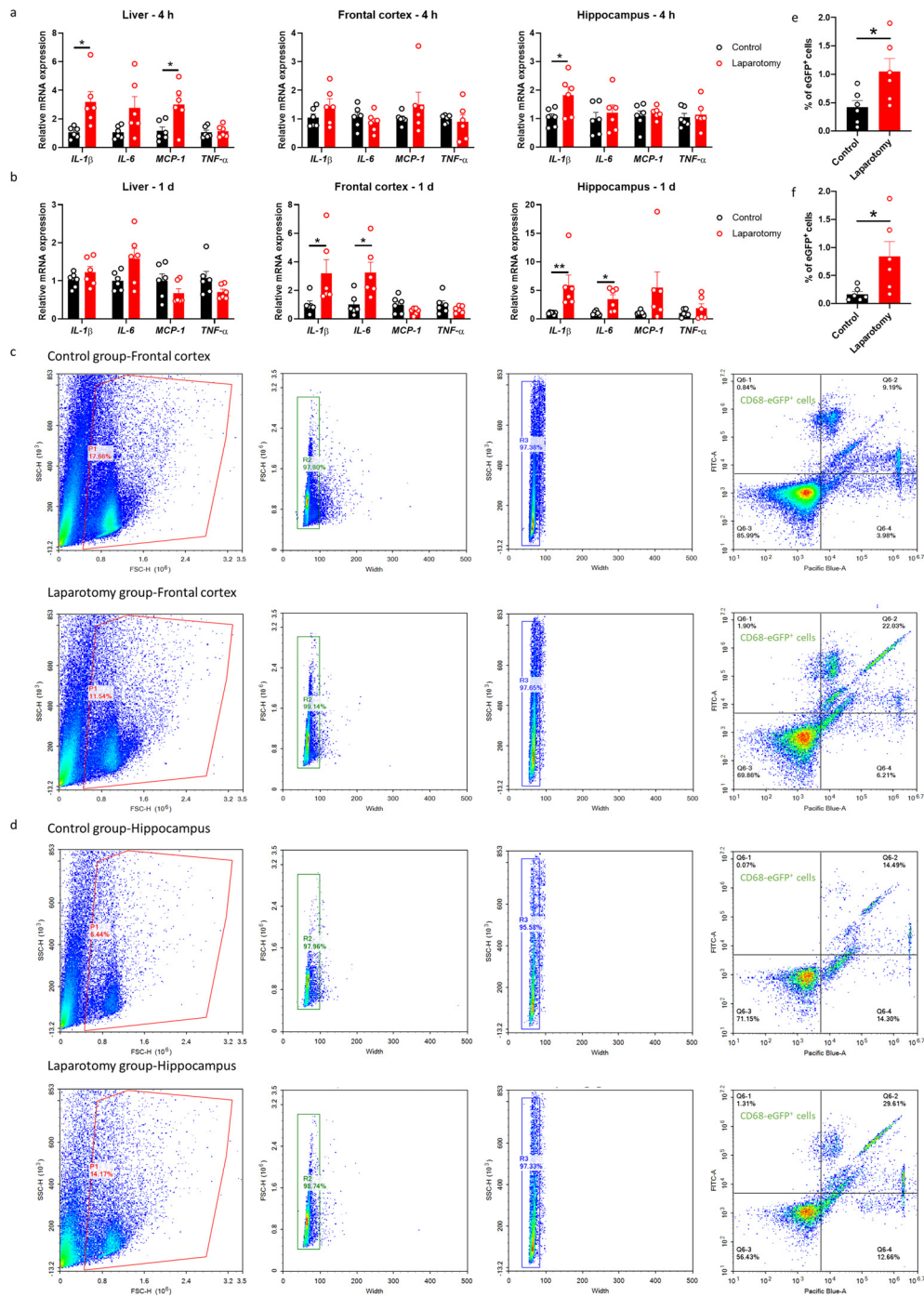


FIGURE 2

Laparotomy induced systemic inflammation and neuroinflammation. Relative cytokine mRNA expression levels were measured in the liver, frontal cortex, and hippocampus of C57BL/6J mice at (A) 4 h and (B) 1 day after laparotomy. Representative flow cytometry plots illustrating the increase in CD68-eGFP⁺ cells in the (C) frontal cortex and (D) hippocampus of the CD68-eGFP mice on postoperative day 14. Morphological gating strategy refers to dot plot SSC-H versus FSC-H to eliminate debris and aggregates in the (C) frontal cortex and (D) hippocampus of the control and laparotomy groups. Doubles are excluded by plotting FSC-H versus width and SSC-H versus width. Proportion of CD68-eGFP⁺ cells (labeled with eGFP) and cell viability (labeled with DAPI) were determined by flow cytometry with FITC and Pacific Blue channel respectively. The data generated are plotted in two-dimensional dot plots in which FITC-A versus Pacific-Blue-A. A four-quadrant gate was established: Q1) live, CD68-eGFP⁺ cells (FITC positive/Pacific blue negative); Q2) dead, CD68-eGFP⁺ cells (FITC positive/Pacific blue positive); Q3) live cells without CD68 expression (FITC negative/Pacific blue negative); and Q4, dead cells without CD68 expression (FITC negative/Pacific blue positive). Percentage of CD68-eGFP⁺ cells in the (E) frontal cortex and (F) hippocampus of the control and laparotomy groups. n = 6 per group. Data are expressed as mean \pm S.E.M. Differences were assessed by unpaired two-tailed Student's t-test as follows: **p* < 0.05 and ***p* < 0.01 compared with the control group.

molecule 1 (Iba1), to further confirm whether laparotomy induces activation of microglia. More Iba1⁺ cells were found in both frontal cortex and hippocampus of the laparotomy group when compared to controls (Frontal cortex: $p < 0.05$; CA1 and CA3: $p < 0.001$; DG: $p < 0.01$; **Figure 3**). Increased fluorescence intensity was also observed in the hippocampus following laparotomy ($p < 0.05$; **Figure 3**). Microglial morphology, an important indicator of

neuroinflammation, was further quantified by skeleton analysis (44). Reduced total endpoints or/and shorter process length per microglial cell were observed in the frontal cortex and the CA1 and DG of the hippocampus of the laparotomy group compared with those of the control counterpart ($p < 0.05$; **Figures 3B, D, H**). This finding revealed that microglia were de-ramified following laparotomy.

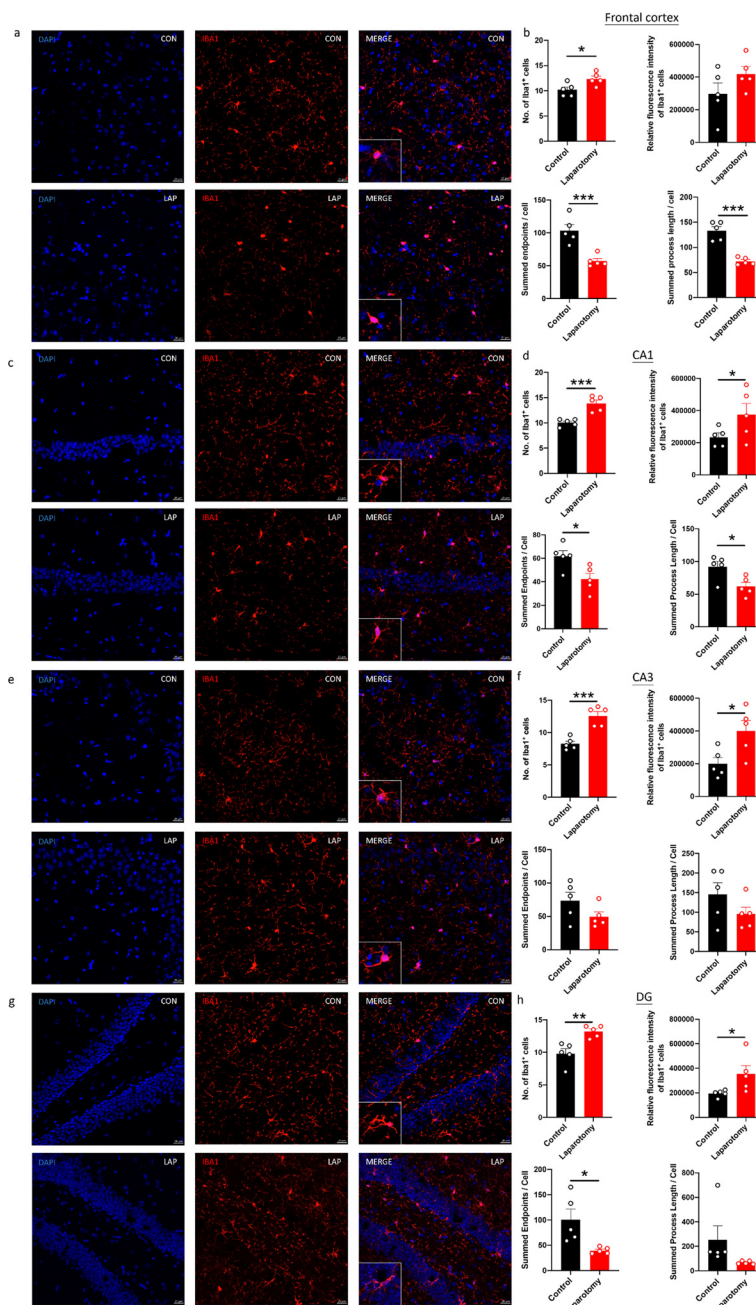


FIGURE 3

Laparotomy induced activation of microglia in the frontal cortex and hippocampus after laparotomy. Representative confocal images of the immunohistochemical staining of DAPI, and Iba1 in the (A) frontal cortex, (C) cornu ammonis (CA) 1, (E) CA3, and (G) dentate gyrus (DG) of the hippocampus sections from CD68-eGFP mice of the control and laparotomy groups on postoperative day 14. Number of Iba1 positive cells, relative fluorescence intensity of Iba1 positive cells, total number of endpoints per Iba1 positive cell, and summed process length per Iba1 positive cell in the (B) frontal cortex, (D) CA 1, (F) CA3, and (H) DG of the hippocampus sections were quantified. $n = 5$ per group. Data are expressed as mean \pm S.E.M. Differences were assessed by unpaired two-tailed Student's t-test denoted as follows: * $p < 0.05$, ** $p < 0.01$ and *** $p < 0.001$ compared with the control group.

3.2 Changes of body weight and cognitive performance in wild-type mice following laparotomy

Body weights were recorded throughout the experiment. Wild-type laparotomy mice exhibited notable weight loss in the first 6 days following surgery ($p < 0.05$; Figure 4A) but no remarkable decreases thereafter.

A series of behavioral tests was performed to study whether laparotomy affects cognitive functions in the wild-type mice. During the OFT, total distance traveled and central area exploration time were similar between laparotomy and control groups (Figures 4B, C). This finding implied that laparotomy did not affect the locomotor activity, exploration, or anxiety. NOR then evaluated recognition memory according to the innate preference of mice for novelty (41). On the first day of NOR, both groups of mice spent comparable time exploring the identical objects (Figure 4D). On day 2 of NOR, impaired recognition memory with lower discrimination index was observed in the laparotomy group

versus the controls ($p < 0.05$; Figure 4E). As indicated by the reduced percentage of alternation, impaired spatial working memory was detected in the laparotomy group when compared to the control ($p < 0.05$; Figure 4G) during SYM with similar total number of entries (Figure 4F). Puzzle box test was adopted to examine the rodent's native problem-solving ability during trial (T) 2, T5, T8, and T11. Additionally, evaluations at the T3, T6, T9, and T12 provided insights into their short-term memory recall, while the T4, T7, T10, and T13 were indicative of their long-term memory function (41). In the habituation task (T1), both groups spent similar time to complete the escape task (Figure 4H). Impaired problem-solving abilities requiring a longer period of time to complete the escape task in T2, T5, and T11 were detected in the laparotomy group compared to controls ($p < 0.05$; Figure 4I). Furthermore, the laparotomy group showed reduced short-term (with increased latency in T12) ($p < 0.05$; Figure 4J) and long-term (with increased latency in T7, T10, and T13) memories when compared to controls (T7 and T13: $p < 0.05$; T10: $p < 0.01$; Figure 4K).

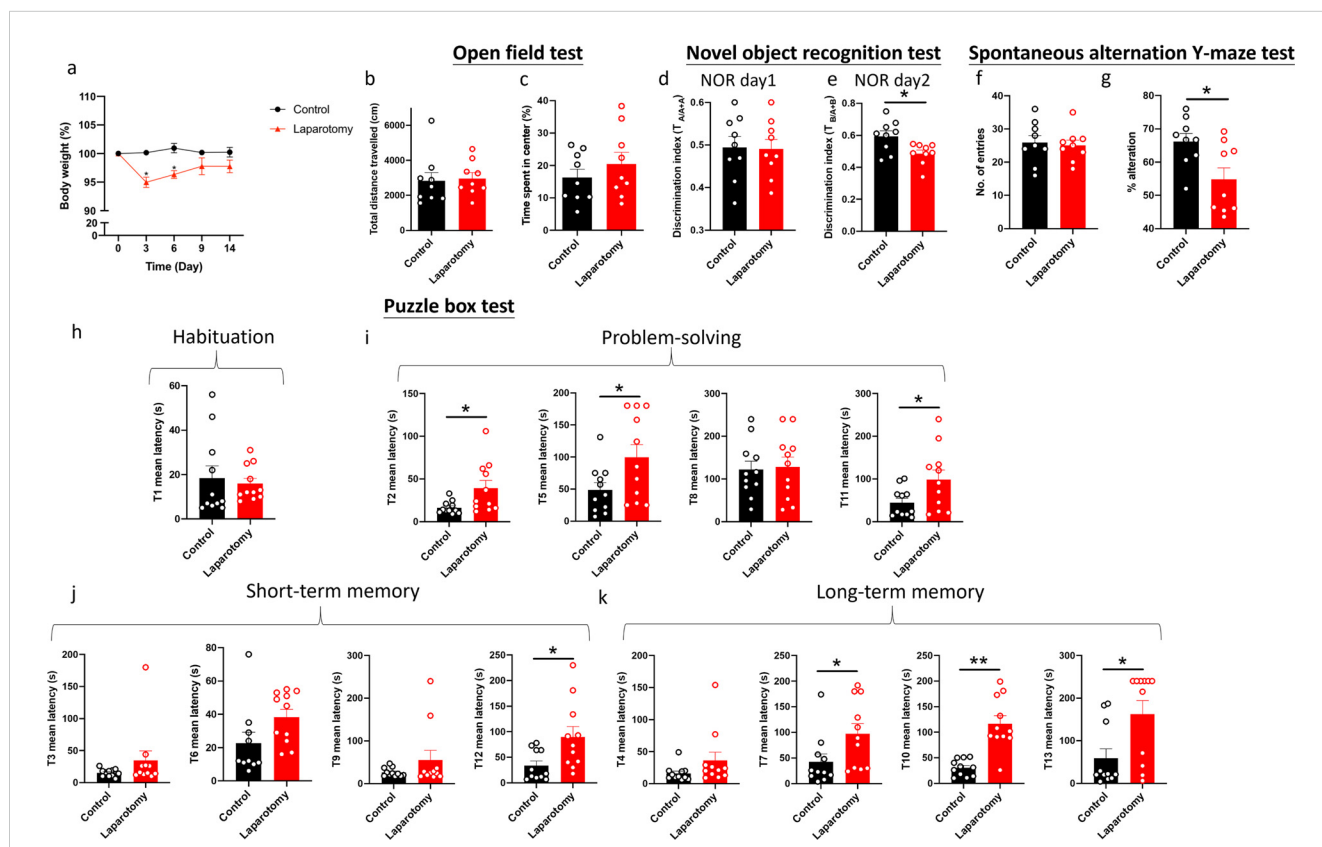


FIGURE 4 Cognitive impairment of C57BL/6J mice following laparotomy. (A) Percentage of the body weight change from baseline of the laparotomy and control groups throughout the postoperative period. (B) Total distance travelled and (C) central duration of mice in the open-field test. (D) Discrimination index, which is the ratio of exploration time of one object to two objects, was measured on the novel object recognition test day 1 (with two identical objects: A +A) and (E) day 2 (with a novel object replaced the familiar one: A+B). (F) Total number of arm entries and (G) percentage of alternation were measured in the spontaneous alternation Y-maze test. In the puzzle box test, the latency time for the mice entering the goal zone in different tasks was measured. All the tasks include (H) task for habituation (T1), (I) tasks for testing problem-solving skills (T2, T5, T8, and T11), and (J) tasks for evaluating short-term (T3, T6, T9, and T12) and (K) long-term memories (T4, T7, T10, and T13) in the puzzle box test. $n = 9-11$ per group. Data are expressed as mean \pm S.E.M. Differences were assessed by unpaired two-tailed Student's t-test denoted as follows: * $p < 0.05$ and ** $p < 0.01$ compared with the control group.

3.3 Knockout of PKR in mice potentially downregulated the up-regulated pro-inflammatory cytokine expressions induced by laparotomy and ameliorated the microglial activation following laparotomy

Given that PKR regulates immune responses, we assessed whether genetic deletion of PKR could abrogate laparotomy-induced inflammation. Two-way ANOVA showed significant effects of laparotomy or/and mouse strain on the pro-inflammatory cytokine expressions in the liver and different brain regions (Supplementary Table S4). Specifically, in the liver, significant effects of laparotomy were observed on the expression of *IL-1 β* ($F(1, 20) = 10.93, p = 0.0035$), *IL-6* ($F(1, 20) = 9.336, p = 0.0062$), *MCP-1* ($F(1, 20) = 12.00, p = 0.0024$), and *TNF- α* ($F(1, 20) = 7.015, p = 0.0154$), while mouse strain also had significant effects on *IL-1 β* ($F(1, 20) = 9.267, p = 0.0064$) and *MCP-1* ($F(1, 20) = 5.718, p = 0.0267$) (Supplementary Table S4). A significant interaction between laparotomy and mouse strain was observed for *TNF- α* ($F(1, 20) = 4.510, p = 0.0464$) (Supplementary Table S4). In the frontal cortex, significant effects of mouse strain were observed on the expression of *IL-1 β* ($F(1, 20) = 18.49, p = 0.0003$), *IL-6* ($F(1, 20) = 8.074, p = 0.0101$), and *MCP-1* ($F(1, 20) = 5.217, p = 0.0334$), but no significant effects of laparotomy or interaction were detected (Supplementary Table S4). In the hippocampus, significant effect of laparotomy was observed on *IL-1 β* expression ($F(1, 20) = 5.983, p = 0.0238$), while no significant effects of mouse strain or interaction were observed (Supplementary Table S4). Bonferroni's *post hoc* tests were performed and showed that *IL-1 β* expression was significantly elevated in liver and hippocampus of the wild-type mice at four hours post-surgery ($p < 0.05$; Figure 5A) but not in the PKR^{-/-} mice after the surgery compared with that in the controls (Figure 5A).

Meanwhile, expression of *IL-1 β* in liver and frontal cortex was significantly reduced in the PKR^{-/-} laparotomy group when compared to the wild-type laparotomy group ($p < 0.05$; Figure 5A). With regard to *MCP-1* expression in the liver, a significant increase was observed in the wild-type mice after laparotomy ($p < 0.05$; Figure 5A) while not in the PKR^{-/-} mice (Figure 5A). Hepatic *TNF- α* expression was significantly elevated in PKR^{-/-} mice after laparotomy compared to PKR^{-/-} controls ($p < 0.05$; Figure 5A); wild-type mice showed no such difference.

On POD 1, two-way ANOVA analysis on POD 1 examined the effects of laparotomy and mouse strain on cytokine expression across different tissues (Supplementary Table S5). In the frontal cortex, significant main effects of laparotomy were observed for *IL-1 β* [$F(1, 20) = 6.049, p = 0.0231$] and *IL-6* [$F(1, 20) = 5.102, p = 0.0352$], along with significant main effects of mouse strain [$F(1, 20) = 9.349, p = 0.0062$] and interaction effects on *IL-6* [$F(1, 20) = 10.08, p = 0.0048$] (Supplementary Table S5). In the hippocampus, significant main effects of laparotomy were found for both *IL-1 β* ($F(1, 20) = 12.93, p = 0.0018$) and *IL-6* ($F(1, 20) = 8.928, p = 0.0073$) (Supplementary Table S5). The liver showed minimal changes, with only an interaction effect on *TNF- α* ($F(1, 20) = 4.923, p = 0.0382$) (Supplementary Table S5). Following these significant ANOVA results, Bonferroni *post hoc* tests revealed that the wild-type laparotomy group revealed a substantial increase in *IL-1 β* and *IL-6* mRNA expression in frontal cortex and hippocampus, compared to the wild-type controls ($p < 0.05$; Figure 5B); no such increases were detected in the PKR^{-/-} laparotomy group. Meanwhile, the PKR^{-/-} laparotomy group showed significantly lower *IL-6* expression in the frontal cortex versus the wild-type laparotomy group ($p < 0.01$; Figure 5B). Between the surgical and control groups for both strains of mice, no remarkable differences in *IL-1 β* , *IL-6*, *MCP-1*, and *TNF- α* mRNA expression were detected in

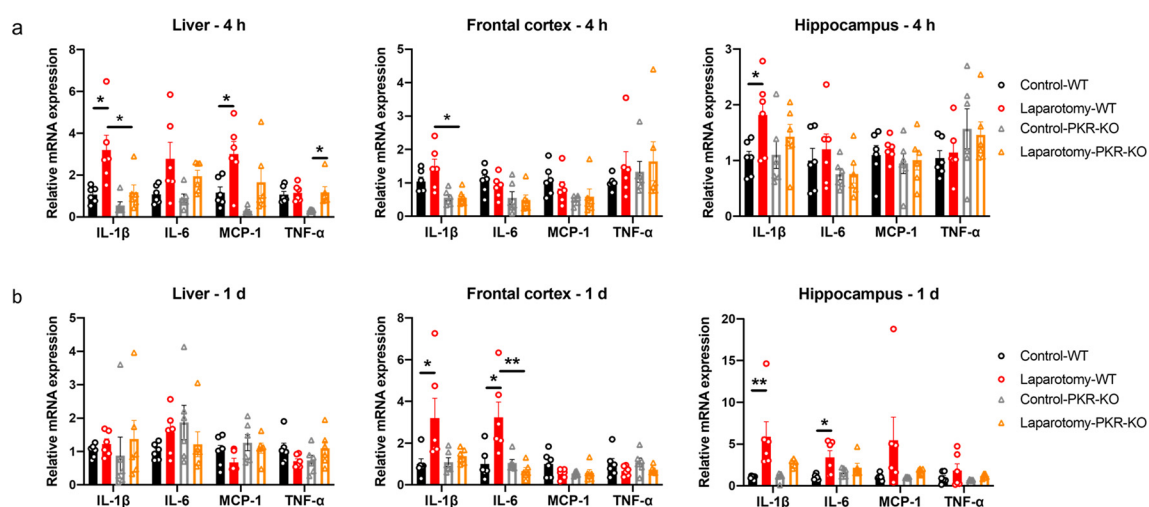


FIGURE 5

Knockout of PKR in mice ameliorated laparotomy-induced peripheral and neural inflammation after surgery. Relative cytokine mRNA expression levels were measured in the liver, frontal cortex, and hippocampus of the C57BL/6J mice and PKR-KO mice at (A) 4 h and (B) 1 day following laparotomy. $n = 6$ per group. Data are expressed as mean \pm S.E.M. Differences were assessed by two-way ANOVA. Bonferroni's *post hoc* tests were performed for the following comparisons: between control and laparotomy treatments within each strain, and between WT and PKR-KO mice under the same treatment condition. * $p < 0.05$ and ** $p < 0.01$ indicate significant differences between indicated groups.

the liver (Figure 5B) and no remarkable alterations in *MCP-1* and *TNF- α* expression were found in frontal cortex and hippocampus (Figure 5B).

We then further investigated whether knockout of PKR could inhibit activation of microglia in the laparotomy model. No observable difference in the number and fluorescence intensity of Iba1⁺ cells in the frontal cortex (Figures 6A, B) and hippocampus was found between the PKR^{-/-} laparotomy group and its control counterpart (Figures 6C–H). Concurrently, laparotomy did not induce morphological changes (total number of endpoints and summed branch lengths) in microglia in the frontal cortex (Figures 6A, B) and hippocampus (Figures 6C–H) of PKR^{-/-} mice compared with those in the control. The PKR^{-/-} mice showed ameliorated neuroimmune responses compared to wild-type mice, indicating the critical role of PKR in regulating neuroinflammation following laparotomy.

3.4 Knockout of PKR in mice ameliorated the cognitive deficits induced by laparotomy

Regardless of the mouse strain, laparotomy resulted in a considerable body weight loss within 3 days ($p < 0.05$; Figure 7A). PKR^{-/-} mice restored weight by day 6, earlier than that of the wild-type mice (on day 9). In the laparotomy group, neither strain of mice lost significant weight after day 9 (Figure 7A). Regarding the open-field test, two-way ANOVA showed that no significant effects of laparotomy, mouse strain, or their interaction were observed on the locomotor activity (total distance travelled) and anxiety level (central duration) (Figures 7B, C, Supplementary Table S6). Similarly, in the NOR test, no significant effect of mouse strain was found on the discrimination index on NOR day 1 (Figure 7D, Supplementary Table S6); however, significant effect of laparotomy was found on NOR day 2 ($F(1, 30) = 6.174, p = 0.0188$), with no significant effects of mouse strain or interaction. Bonferroni *post hoc* tests revealed that laparotomy impaired the recognition memory (reduced discrimination index) of the wild-type mice ($p < 0.05$; Figure 7E) but not that of the PKR^{-/-} mice (Figure 7E). In the SYM, no effects of laparotomy, mouse strain, or interaction were detected for total arm entries (Figure 7F, Supplementary Table S6); while significant effect of laparotomy was found for the percentage of alternation ($F(1, 30) = 3.906, p = 0.0494$) (Supplementary Table S6). Laparotomy impaired the spatial recognition memory (reduced percentage of alternation) of the wild-type mice ($p < 0.05$; Figure 7G) but not that of the PKR^{-/-} mice (Figure 7G).

The puzzle box test was conducted to further assess the rodent's problem-solving skill and short-term and long-term memories. In the puzzle box test, throughout habituation (T1), no significant effects of laparotomy were detected (Figure 7H, Supplementary Table S6); while significant effects of mouse strain were observed in T1 ($F(1, 36) = 23.91, p < 0.0001$), with the PKR^{-/-} mice demonstrated greater latency to enter the goal zone than the wild-type mice ($p < 0.01$; Figure 7H, Supplementary Table S6). In terms of problem-solving ability, significant effects of laparotomy

were detected at several tasks, including T2 ($F(1, 36) = 6.659, p = 0.0141$), T5 ($F(1, 36) = 5.275, p = 0.0277$); notably, in T2 and T11, significant effects of mouse strain (T2 ($F(1, 36) = 15.76, p = 0.0003$); T11: $F(1, 36) = 4.898, p = 0.0333$) were observed, as well as significant interaction between laparotomy and mouse strain in T11 ($F(1, 36) = 5.438, p = 0.0254$) (Supplementary Table S6). In T2, T5 and T11, the wild-type laparotomy mice took longer to solve task T2, T5, and T11 ($p < 0.05$; Figure 7I); while PKR^{-/-} laparotomy mice showed no such delays when compared to their PKR^{-/-} controls (Figure 7I). In T2, the PKR^{-/-} laparotomy mice demonstrated greater latency when compared to the wild-type laparotomy group ($p < 0.05$; Figure 7I); a similar trend was also detected in T11 between the PKR^{-/-} controls and their wild-type control counterpart ($p < 0.05$; Figure 7I). Regarding the short- and long-term memories, significant effects of laparotomy were detected at T7 ($F(1, 36) = 8.585, p = 0.0059$), T10 ($F(1, 36) = 16.75, p = 0.0002$), T12 ($F(1, 36) = 4.249, p = 0.0498$) and T13 ($F(1, 36) = 4.256, p = 0.0464$) (Supplementary Table S6). Laparotomy did not impair the short- and long-term memories of the PKR^{-/-} mice; while the wild-type laparotomy group showed significant impairment (T7, T12, and T13: $p < 0.05$; T10: $p < 0.01$; Figures 7J, K). This result suggested that genetic deletion of PKR could ameliorate the cognitive deficits induced by laparotomy.

3.5 Inhibition of PKR in cholinergic neurons partially ameliorated laparotomy-induced cognitive dysfunctions

rAAV-DIO-PKR-K296R was intracerebroventricularly injected into the right lateral ventricle of the ChAT-IRES-Cre-eGFP mice to inhibit activation of PKR in cholinergic neurons. rAAV expresses a dominant negative form of PKR, that is, PKR-K296R, under the regulation of a double-floxed inverse orientation (DIO) switch (Supplementary Figure S3A). At 4 weeks after the stereotaxic injection of rAAV-DIO-PKR-K296R, the fluorescence intensity of p-PKR (T446) signal and the fluorescence ratio of p-PKR to the eGFP signal were reduced in the rAAV-DIO-PKR-K296R-treated group when compared to the saline-treated control ($p < 0.05$; Supplementary Figure S3B, C). Therefore, in ChAT-IRES-Cre-eGFP mice, the expression of PKR-K296R effectively suppressed the activation (phosphorylation) of PKR.

At 4 weeks following stereotaxic injection, mice were randomized into four groups: saline-treated control group given only sevoflurane (SAL-CON), saline-treated group subjected to laparotomy (SAL-LAP), AAV-treated group given only sevoflurane (AAV-CON), and AAV-treated group subjected to laparotomy (AAV-LAP). Within 3 days after laparotomy, the SAL-LAP and AAV-LAP groups lost significant weight ($p < 0.05$; Figure 8A), similar to the wild-type and PKR^{-/-} mice. On POD 6, their body weight returned to normal, and no remarkable difference was detected across all the groups (Figure 8A).

Different behavioral tests were conducted to investigate the effects of inhibiting PKR in cholinergic neurons on cognition following laparotomy. In the open-field test, no significant effects of laparotomy, AAV treatment, or their interaction were observed

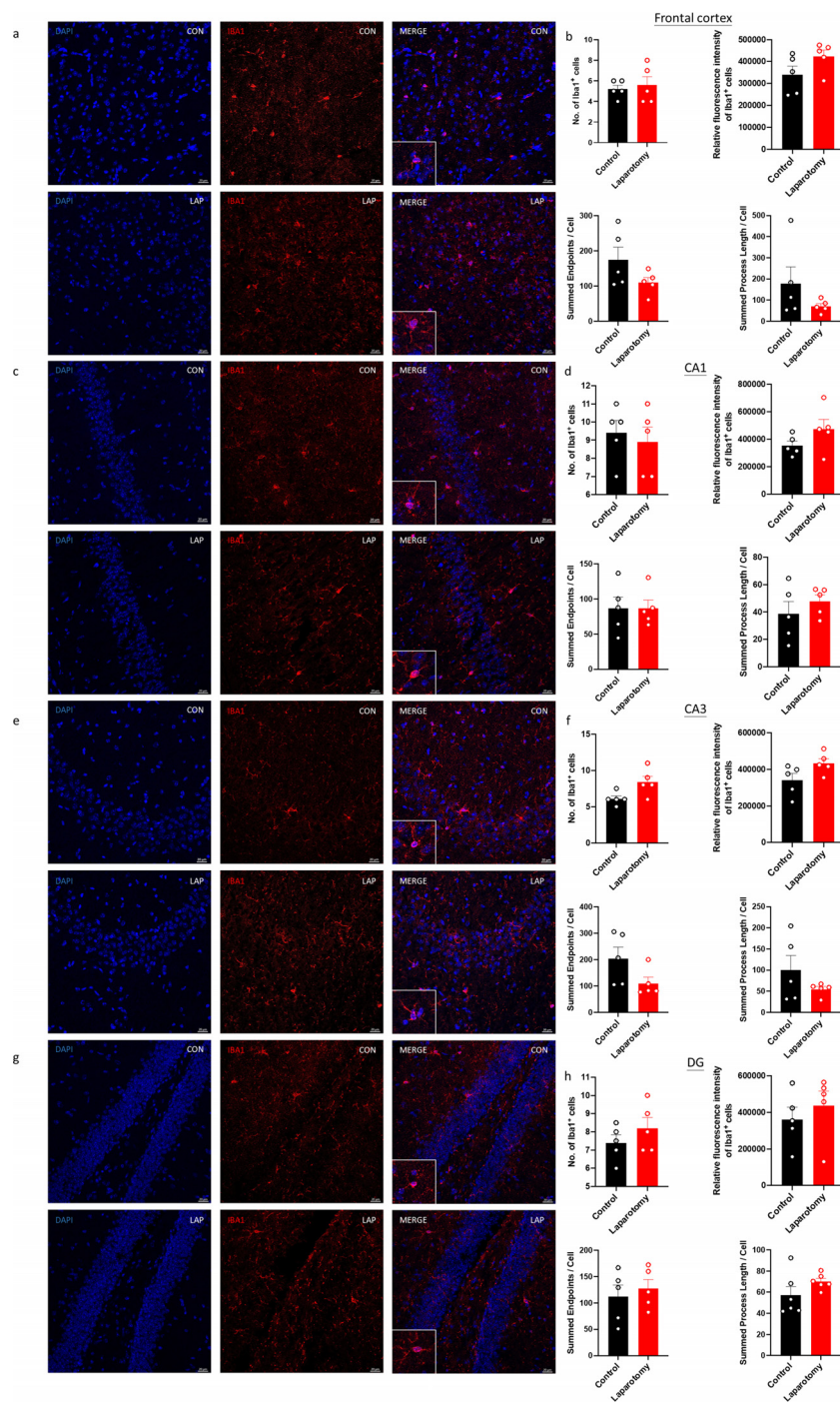
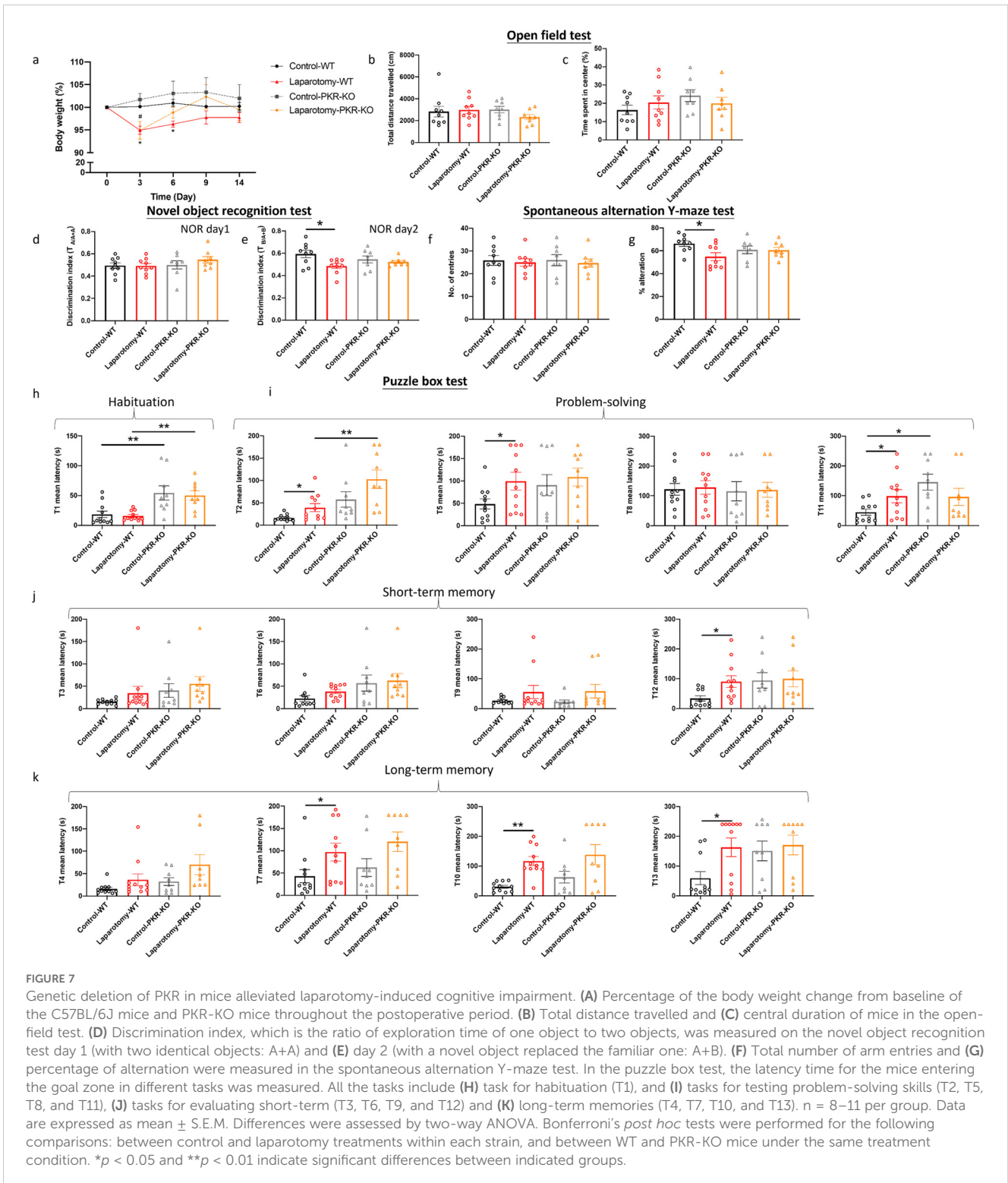


FIGURE 6 Knockout of PKR in mice ameliorated activation of microglia in the frontal cortex and hippocampus following laparotomy. Representative confocal images of the immunohistochemical staining of DAPI and Iba1 in the (A) frontal cortex, (C) cornu ammonis (CA) 1, (E) CA3, and (G) dentate gyrus (DG) of the hippocampus sections from PKR-KO mice of the control and laparotomy groups on postoperative day 14. Number of Iba1 positive cells, relative fluorescence intensity of Iba1 positive cells, total number of endpoints per Iba1 positive cell, and summed process length per Iba1 positive cell in the (B) frontal cortex, (D) CA1, (F) CA3, and (H) DG of the hippocampus sections were quantified. n = 5 per group. Data are expressed as mean ± S.E.M. Differences were assessed by unpaired two-tailed Student's t-test.

on locomotor activity (total distance travelled) and anxiety level (central duration) (Figures 8B, C, Supplementary Table S7). In the SYM test, significant effect of laparotomy was found for the percentage of alternation ($F(1, 25) = 4.974, p = 0.0349$); specifically, impaired spatial memory with lower percentage of

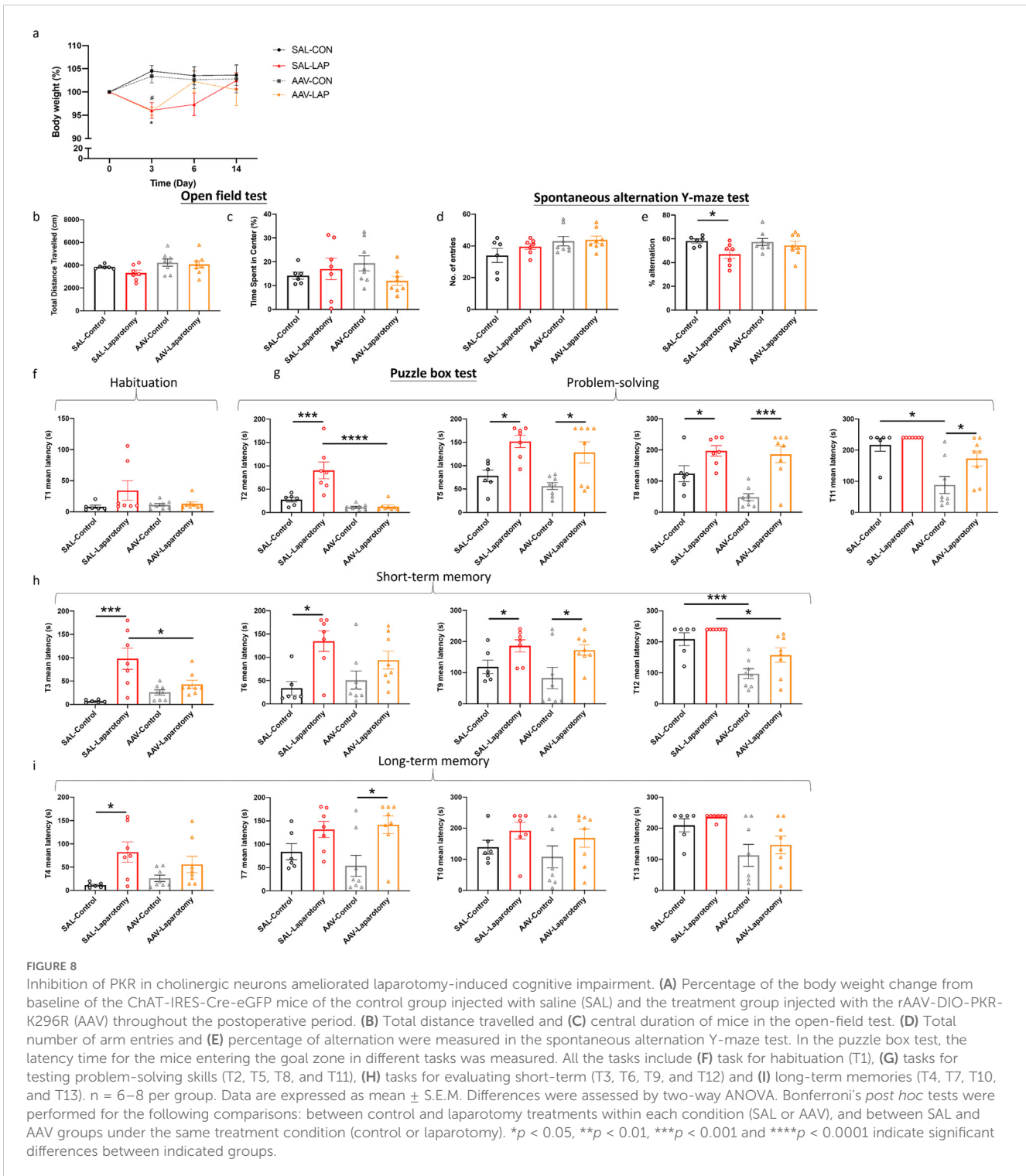
alternation was detected in the SAL-LAP group when compared to the SAL-CON ($p < 0.05$; Figure 8E); AAV-treated mice showed no such difference. While a significant main effect of AAV treatment on total arm entries was detected ($F(1, 25) = 5.277, p = 0.0303$), Bonferroni *post hoc* comparisons revealed no



significant differences between specific groups (Figure 8D). Our findings suggested that inhibiting PKR in cholinergic neurons could alleviate the spatial working memory deficits induced by laparotomy.

Considering the habituation task (T1) of the puzzle box test, no effects of laparotomy, AAV treatment, or interaction were detected (Supplementary Table S7). All the groups of mice completed the

escape task in about the same amount of time (Figure 8F). In general, significant main effects of laparotomy were observed at multiple tasks (T2: $F(1, 25) = 12.33, p = 0.0017$; T3: $F(1, 25) = 19.05, p = 0.0002$; T4: $F(1, 25) = 11.47, p = 0.0023$; T5: $F(1, 25) = 22.01, p < 0.0001$; T6: $F(1, 25) = 13.61, p = 0.0011$; T7: $F(1, 25) = 11.66, p = 0.0022$; T8: $F(1, 25) = 25.35, p < 0.0001$; T9: $F(1, 25) = 9.854, p = 0.0043$; T11: $F(1, 25) = 5.876, p = 0.0229$ and T12: $F(1, 25) = 6.460,$



$p = 0.0176$) and significant main effects of AAV treatment were observed at various tasks (T2: $F(1, 25) = 26.39, p < 0.0001$; T8: $F(1, 25) = 4.249, p = 0.0498$; T11: $F(1, 25) = 19.59, p = 0.0002$ and T12: $F(1, 25) = 29.08, p < 0.0001$; T13: $F(1, 25) = 12.00, p = 0.0019$) (Supplementary Table S7). Significant interactions between laparotomy and AAV treatment were detected at T2 ($F(1, 25) = 11.10, p = 0.0027$) and T3 ($F(1, 25) = 8.795, p = 0.0066$) (Supplementary Table S7).

In terms of problem-solving ability, contrasting behaviors were observed. In the T2 task, Bonferroni *post hoc* tests revealed that the SAL-LAP group demonstrated increased latency when compared to the SAL-CON ($p < 0.001$; Figure 8G); no notable difference was found in the AAV-treated group (Figure 8G). Meanwhile, the AAV-LAP group solved the T2 task faster than the SAL-LAP group ($p < 0.0001$; Figure 8G). This result revealed that inhibiting PKR in cholinergic neurons could improve the cognitive functions of mice

in the T2 task following laparotomy. In the T5 and T8 task, however, the AAV-treated and saline-treated mice showed increased latency time following laparotomy when compared to their control counterparts ($p < 0.05$; **Figure 8G**). With respect to T11 task, the AAV-LAP group demonstrated a significant prolonged latency when compared to the AAV-CON ($p < 0.05$; **Figure 8G**). Meanwhile, the AAV-CON group demonstrated better problem-solving skills than the SAL-CON ($p < 0.05$; **Figure 8G**).

Regarding short-term memory, consistent results were observed in the T3 and T6 tasks (**Figure 8H**). When compared with the SAL-CON group, the SAL-LAP mice showed impaired short-term memory with increased latency to solve the T3 ($p < 0.001$; **Figure 8H**) and T6 tasks ($p < 0.05$; **Figure 8H**). Such differences were not detected in the AAV-treated groups. In the T3 task, the AAV-LAP group escaped faster than the SAL-LAP group ($p < 0.05$; **Figure 8H**). This finding indicated that inhibiting PKR in cholinergic neurons helped alleviate the short-term memory deficits induced by laparotomy. However, for the T9 task, the AAV-treated and saline-treated mice showed increased latency following laparotomy when compared to the controls ($p < 0.05$; **Figure 8H**). Moreover, the AAV-treated group demonstrated reduced latency for the T12 task compared with their saline-treated counterpart ($p < 0.05$; **Figure 8H**). Therefore, inhibition of PKR in cholinergic neurons could improve short-term memory.

For long-term memory, contrasting behaviors were observed in the T4 and T7 tasks. In the T4 task, the SAL-LAP group showed impairment ($p < 0.05$; **Figure 8I**); AAV-treated mice showed no such difference (**Figure 8I**). In T7 task, a noticeable change was observed only in the AAV-treated groups, with increased latency to solve the task by the AAV-LAP group compared with the AAV-CON group ($p < 0.05$; **Figure 8I**) but not in the saline-treated groups (**Figure 8I**). No significant difference for all the tasks testing long-term memory (T4, T7, T10, and T13 tasks) was observed between the AAV-treated and SAL-treated groups. Therefore, no concrete conclusions concerning the influence of PKR inhibition in cholinergic neurons on long-term memory could be drawn.

3.6 Inhibition of PKR in cholinergic neurons alters glucose metabolism in the frontal cortex in a laparotomy model

MS-based targeted metabolomics was performed to examine the effects of PKR inhibition in cholinergic neurons on brain glucose metabolism. Distinct clustering was observed between the SAL-LAP and AAV-CON groups (**Figures 9A, B**). The heatmap depicted the changes of quantified metabolites including tricarboxylic acids and glycolysis intermediates in the frontal cortex across all the groups (**Figure 9C**). Two-way ANOVA revealed that significant effects of laparotomy on several brain glucose metabolites. While no significant effects of laparotomy, AAV treatment, or their interaction were observed for glucose levels (**Figure 9D**, **Supplementary Table S8**), laparotomy significantly affected phosphoenolpyruvate ($F(1, 12) = 7.846$, $p = 0.0160$), succinate ($F(1, 12) = 4.795$, $p = 0.0490$), and 6-phosphogluconate ($F(1, 12) = 9.743$, $p = 0.0088$) (**Supplementary Table S8**).

Additionally, significant effects of AAV treatment were observed on phosphoenolpyruvate ($F(1, 12) = 6.562$, $p = 0.0249$) and 6-phosphogluconate ($F(1, 12) = 14.65$, $p = 0.0024$) (**Supplementary Table S8**). However, no significant interactions were detected for any of the metabolites (**Supplementary Table S8**). These results suggest that laparotomy and AAV treatment independently affect specific glucose metabolites. Bonferroni *post hoc* tests revealed that laparotomy significantly reduced the level of phosphoenolpyruvate in the SAL-LAP group when compared to the control counterpart ($p < 0.05$; **Figure 9E**). However, no notable difference in phosphoenolpyruvate level was detected in the AAV-treated group following laparotomy. Therefore, inhibiting PKR in cholinergic neurons could ameliorate the laparotomy-induced changes in phosphoenolpyruvate level. Similarly, laparotomy reduced the succinate level in the SAL-treated mice ($p < 0.05$; **Figure 9F**) but not in the AAV-treated group (**Figure 9F**). Apart from the laparotomy-induced changes in glycolysis intermediates, inhibition of PKR in cholinergic neurons significantly elevated the level of 6-phosphogluconate in the AAV-CON group when compared to that in the SAL-CON group ($p < 0.01$; **Figure 9G**), suggesting that PKR inhibition in cholinergic neurons could alter brain energy metabolism. Altogether, inhibition of PKR in cholinergic neurons of ChAT-IRES-Cre-eGFP mice attenuated the laparotomy-induced brain glucose hypometabolism.

4 Discussion

Neuroinflammation is a major cause of cognitive impairment in PND. In this study, we employed a clinically relevant mouse model of laparotomy to induce peripheral and neural inflammation and further demonstrate the regulatory role of PKR in systemic inflammation-induced neuroinflammation and cognitive dysfunctions.

Regarding the laparotomy model, systemic and neural immune responses developed rapidly after the surgery. In theory, laparotomy results in peritoneal air exposure (45, 46), tissue injury, and gut mucosa barrier damage, resulting in increased inflammatory mediators and gut bacteria/endotoxin translocation to the circulation, contributing to systemic inflammation (47, 48). Our study found a significant elevation in the cytokine mRNA expression of liver (*IL-1 β* and *MCP-1*) and brain tissues (*IL-1 β*) at four hours after laparotomy (**Figure 2A**). On POD 1, laparotomy triggered a significant upregulation of *IL-1 β* and *IL-6* expression in frontal cortex and hippocampus (**Figure 2B**). The cytokine, IL-1 β , plays an important role in neuroinflammation and pathogenesis of AD (49) and PD (50). Through activating nuclear factor κ B (NF- κ B), IL-1 β promotes the upregulation of proinflammatory cytokines including IL-6 and TNF- α (51). This finding may partially explain the increased *IL-6* expression in the brain of the laparotomy group on POD 1 (**Figure 2B**). However, the induced systemic inflammation is relatively transient, with proinflammatory cytokine expression levels in the liver returning to normal on POD 1 (**Figure 2B**). Therefore, a transient systemic inflammation is already sufficient to induce neuroinflammation as evidenced by the persistent microgliosis revealed by flow cytometry (**Figures 2C–F**) and confocal imaging (**Figure 3**) on POD 14. Our findings are also consistent with a prior study that demonstrated

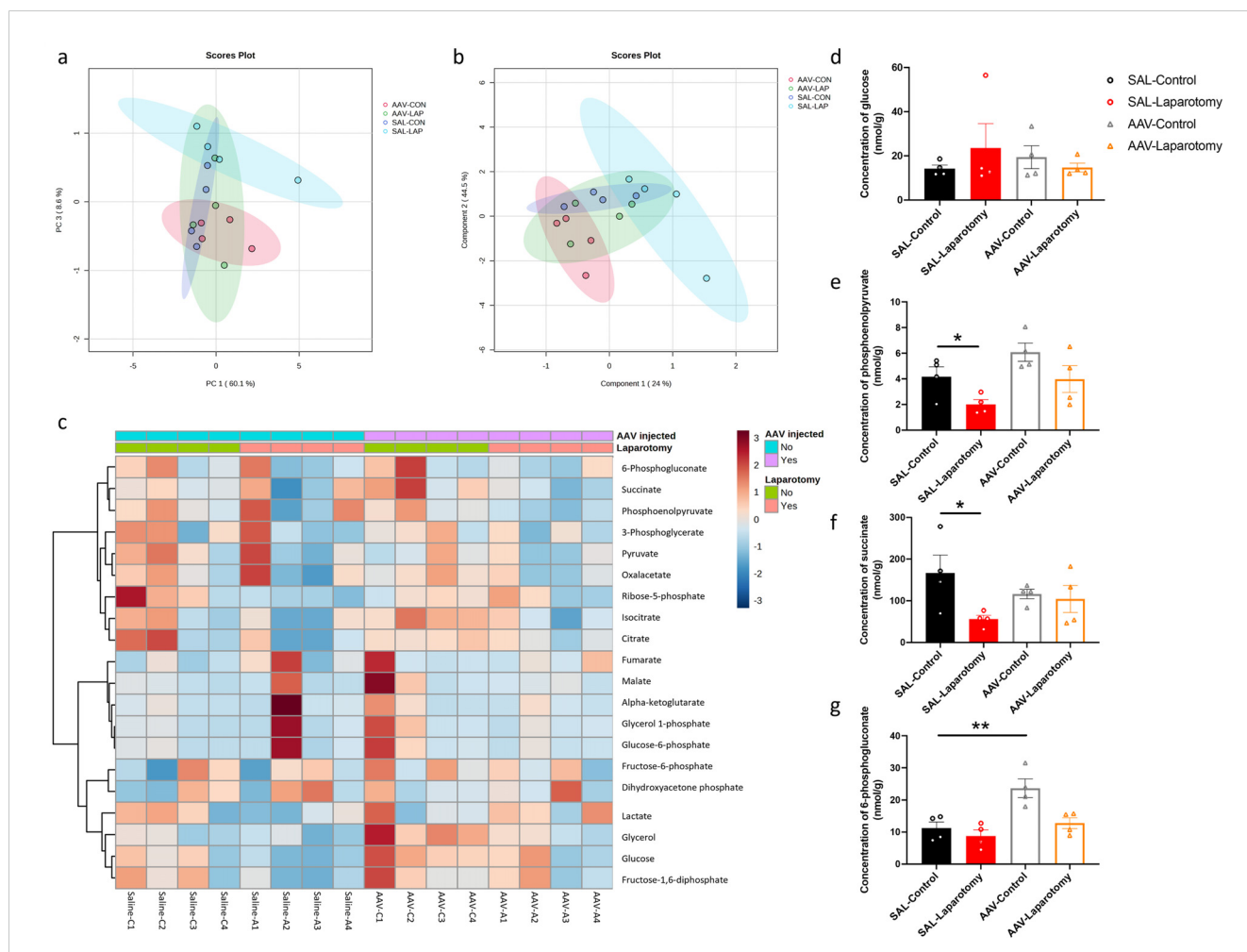


FIGURE 9 Inhibition of PKR in cholinergic neurons ameliorated laparotomy-induced changes in glucose metabolism in the frontal cortex. Two-dimensional score plots using the (A) principal component analysis (PCA) and (B) partial least squares discriminant analysis (PLS-DA). (C) Heatmap of the metabolites involved in central carbon metabolism in the frontal cortex of the ChAT-IRES-Cre-eGFP mice injected with saline (SAL) or rAAV-DIO-PKR-K296R (AAV). Both groups of mice were then randomly assigned into the laparotomy and control groups. The effects of AAV treatment and laparotomy on glucose metabolism were analyzed using gas chromatography–tandem mass spectrometry (GC-MS/MS). The column represents the samples, and the row displays the glucose metabolites. The heatmap scale ranges from -3 to 3 . The brightness of each color corresponded to the magnitude of the \log_2 fold change of the measured metabolites. Concentration of (D) glucose, (E) phosphoenolpyruvate, (F) succinate, and (G) 6-phosphogluconate were quantified in nmol/g, $n = 4$ per group. Data are expressed as mean \pm S.E.M. Differences were assessed by two-way ANOVA. Bonferroni's *post hoc* tests were performed for the following comparisons: between control and laparotomy treatments within each condition (SAL or AAV), and between SAL and AAV groups under the same treatment condition (control or laparotomy). * $p < 0.05$ and ** $p < 0.01$ indicate significant differences between indicated groups.

significant microglial activation in frontal cortex and hippocampus following laparotomy (12). Beyond the microglial activation, cognitive deficits (Figure 4) were also detected in the wild-type laparotomy model mice. Therefore, the laparotomy model is a viable and relevant paradigm for studying systemic inflammation-triggered neuroimmune response and cognitive dysfunction.

Our study is the first to show that genetic deletion of PKR could alleviate laparotomy-induced peripheral and neural inflammation, as well as downregulate the increased expression of *IL-1 β* and *IL-6* in liver, frontal cortex, and hippocampus following laparotomy (Figures 5A, B). Since PKR plays a critical role in *IL-1 β* activation, PKR knockout can help prevent pro-*IL-1 β* from cleaving into *IL-1 β* . These findings were consistent with other previous studies showing that PKR could attenuate inflammation by regulating inflammasome activation (27) and various inflammatory

pathways including TNF (52), p38 MAPK (24), and NF- κ B/I κ B signaling pathway (53). PKR inhibition prevented I κ B and NF- κ B activation and decreased *IL-1 β* expression in primary murine mixed neuron–astrocyte–microglia co-culture model (53) and RAW264.7 macrophages (22). Subsequently, the reduced *IL-1 β* expression further downregulated *IL-6* expression by preventing the activation of NF- κ B. Four hours following surgery, a significant elevation was found in *TNF- α* expression in the liver of the PKR^{-/-} laparotomy group but not in their wild-type counterpart (Figure 5A). However, no notable difference was detected between the PKR^{-/-} and wild-type laparotomy groups. Similar findings were also observed in our earlier investigation, which demonstrated a significant elevation in *TNF- α* expression in the hippocampus of the PKR^{-/-} mice after *Escherichia coli* challenge but not in their wild-type control counterpart (17). Indeed, PKR is involved in TNF-

dependent activation of c-Jun N-terminal kinase (JNK), NF- κ B and protein kinase B. Meanwhile, knockout of PKR could abrogate the TNF-induced activation of the above signaling pathways. Therefore, the PKR^{-/-} laparotomy mice may tend to highly express *TNF- α* to activate the downstream pathways. Our study has taken a significant step beyond previous research. Although previous works showed that genetic deletion of PKR in mice can prevent activation of microglia following intraperitoneal injection of LPS (18), we demonstrated that PKR also alleviates neuroinflammation induced by sterile systemic inflammation as evidenced by the suppressed laparotomy-induced microglial activation in frontal cortex and hippocampus of PKR^{-/-} mice (Figures 5, 6). Therefore, PKR regulates the activation of microglia/macrophages. Since PKR is critical for LPS-induced inducible nitric oxide synthase expression (54), it is responsible for the macrophage inflammatory response by regulating the production of a proinflammatory factor, nitric oxide (55). Moreover, PKR is necessary for the dsRNA-induced activation of macrophages (22). All the aforementioned studies supported the role of PKR in activation of microglia/macrophages. Furthermore, knockout of PKR in mice could rescue the laparotomy-triggered impairment of problem-solving ability, spatial working memory, and short-term and long-term memories in mice (Figures 7E, G, I–K).

Another novel finding of this project is that inhibition of PKR in cholinergic neurons could rescue the laparotomy-induced cognitive deficits. The cholinergic system is selected for investigation because it is not only essential for cognition but also regulates inflammation through the cholinergic anti-inflammatory pathway (56), which connects systemic inflammation and neuroinflammation. This study also demonstrated that inhibition of PKR in cholinergic neurons could alleviate the laparotomy-induced impairment of short-term and spatial working memory (Figures 8E, H). However, this intervention could not rescue the laparotomy-induced impairment of problem-solving skills, and the long-term memory of mice was also worsened in a certain task (Figures 8G, I). These neuron-specific effects of PKR on cognition during inflammation extend beyond its immune regulatory roles. A previous study showed that PKR inhibition could improve cortex-dependent memory consolidation in rats and mice (57). Meanwhile, PKR^{-/-} mice demonstrated enhanced conditioned taste aversion memory when compared with their wild-type control (57); while PKR activation could impair hippocampal late-phase LTP and memory consolidation in PKR recombinant mice (58). All the abovementioned studies supported the crucial role of PKR in regulating cognitive functions. Our research highlights PKR as a potential key target in treating inflammation-induced short-term and spatial working memory, opening up promising possibilities for future therapeutic approaches focusing on PKR modulation.

We observed that laparotomy could lead to brain glucose hypometabolism, characterized by a reduction in glycolysis and citric acid cycle intermediates (phosphoenolpyruvate and succinate) (Figure 9). Such alterations, particularly brain glucose hypometabolism, are hallmarks of neurodegenerative diseases including AD and PD in their preclinical stages (34, 35). The observed changes in metabolic pathways following laparotomy may represent an early manifestation of metabolic reprogramming that

precedes or contributes to cognitive dysfunction. Progressive reduction in brain glucose metabolism positively correlates with amyloid load and cognitive decline in patients with early AD or PD suffering from mild cognitive impairment (35, 59, 60). AD patients showed reduced concentrations of glycolytic intermediates including phosphoenolpyruvate in cerebrospinal fluid (61). By contrast, administering succinate into the brain by retrodialysis could improve the brain reduced/oxidized nicotinamide adenine dinucleotide redox state (62) and brain energy metabolism in patients suffering from traumatic brain injury (63). All of the abovementioned studies established a close association between brain glucose metabolism and cognition.

Our study unraveled the novel role of PKR in regulating brain glucose metabolism in the laparotomy model. Blocking PKR in cholinergic neurons could rescue the laparotomy-induced alterations in glucose metabolism in the frontal cortex on POD 14 (Figures 9E, F). PKR regulates glucose homeostasis (30) and induces insulin resistance (36, 64). Increased eIF2 α phosphorylation is a hallmark of insulin resistance and obesity (36, 37, 64). Under metabolic and obesity-induced stress, PKR could form a complex with TAR RNA-binding protein (TRBP), activating JNK (30). Inhibiting TRBP in the liver could improve insulin sensitivity, glucose metabolism, and alleviate inflammation (30). The interaction between PKR and TRBP links metabolism to inflammatory signaling regulation. However, no prior study has examined the effect of blocking PKR in the brain on glucose metabolism. Our findings supported that PKR in cholinergic neurons play a critical role in modulating glucose metabolism. Further study to unveil the underlying regulatory networks is warranted.

5 Conclusions

The laparotomy model was a stable and viable model for studying neuroimmune responses triggered by sterile systemic inflammation as evidenced by microgliosis and cognitive dysfunction. By genetic deletion of PKR, we demonstrated the critical role of PKR in regulating peripheral and neural inflammation. Knockout of PKR could help alleviate neuroimmune responses and cognitive impairment induced by laparotomy. Furthermore, inhibition of PKR in the cholinergic neurons of the laparotomy mice rescued the laparotomy-induced changes in brain glucose metabolism and alleviated laparotomy-induced impairments of short-term and spatial working memory cognitive functions. On the basis of our combined findings, PKR could be a pharmacological target for treating systemic inflammation-induced neuroinflammation and cognitive deficits.

Data availability statement

The original contributions presented in the study are publicly available. This data can be found here: <https://doi.org/10.6084/m9.figshare.26385013.v2>.

Ethics statement

The animal study was approved by Department of Health of the Hong Kong SAR government and the Committee on the Use of Live Animals in Teaching and Research of the University of Hong Kong. The study was conducted in accordance with the local legislation and institutional requirements.

Author contributions

W-YC: Conceptualization, Data curation, Formal analysis, Investigation, Methodology, Writing – original draft, Writing – review & editing. X-ZL: Investigation, Writing – original draft, Formal analysis. ML: Investigation, Methodology, Writing – review & editing. Y-SH: Writing – review & editing. RC: Conceptualization, Funding acquisition, Project administration, Resources, Supervision, Validation, Writing – review & editing.

Funding

The author(s) declare that financial support was received for the research, authorship, and/or publication of this article. This study is supported by General Research Fund (17123217).

Acknowledgments

The study is partly supported by The Bingei and L & T Charitable Foundation Professorship in Dementia Research. We

References

- Hoogland I, Houbolt C, van Westerloo DJ, van Gool WA, van de Beek D. Systemic inflammation and microglial activation: systematic review of animal experiments. *J Neuroinflammation*. (2015) 12:1–13. doi: 10.1186/s12974-015-0332-6
- Lopez-Rodriguez AB, Hennessy E, Murray CL, Nazmi A, Delaney HJ, Healy D, et al. Acute systemic inflammation exacerbates neuroinflammation in Alzheimer's disease: IL-1 β drives amplified responses in primed astrocytes and neuronal network dysfunction. *Alzheimers Dement*. (2021) 17:1735–55. doi: 10.1002/alz.12341
- Wang RPH, Ho YS, Leung WK, Goto T, Chang RCC. Systemic inflammation linking chronic periodontitis to cognitive decline. *Brain Behav Immun*. (2019) 81:63–73. doi: 10.1016/j.bbi.2019.07.002
- Heneka MT, Carson MJ, El Khoury J, Landreth GE, Brosseron F, Feinstein DL, et al. Neuroinflammation in alzheimer's disease. *Lancet Neurol*. (2015) 14:388–405. doi: 10.1016/S1474-4422(15)70016-5
- Hirsch EC, Hunot S. Neuroinflammation in Parkinson's disease: a target for neuroprotection? *Lancet Neurol*. (2009) 8:382–97. doi: 10.1016/S1474-4422(09)70062-6
- Philips T, Robberecht W. Neuroinflammation in amyotrophic lateral sclerosis: role of glial activation in motor neuron disease. *Lancet Neurol*. (2011) 10:253–63. doi: 10.1016/S1474-4422(11)70015-1
- Fu R, Shen Q, Xu P, Luo JJ, Tang Y. Phagocytosis of microglia in the central nervous system diseases. *Mol Neurobiol*. (2014) 49:1422–34. doi: 10.1007/s12035-013-8620-6
- Kempuraj D, Thangavel R, Selvakumar GP, Zaheer S, Ahmed ME, Raikwar SP, et al. Brain and peripheral atypical inflammatory mediators potentiate neuroinflammation and neurodegeneration. *Front Cell Neurosci*. (2017) 11:216. doi: 10.3389/fncel.2017.00216
- Streit WJ, Mrazek RE, Griffin WST. Microglia and neuroinflammation: a pathological perspective. *J Neuroinflammation*. (2004) 1:14. doi: 10.1186/1742-2094-1-14
- Varvel NH, Neher JJ, Bosch A, Wang W, Ransohoff RM, Miller RJ, et al. Infiltrating monocytes promote brain inflammation and exacerbate neuronal damage after status epilepticus. *Proc Natl Acad Sci USA*. (2016) 113:E5665. doi: 10.1073/pnas.1604263113
- Evered L, Silbert B, Knopman DS, Scott DA, DeKosky ST, Rasmussen LS, et al. Recommendations for the nomenclature of cognitive change associated with anaesthesia and surgery-2018. *Anesthesiology*. (2018) 129:872–9. doi: 10.1097/aln.0000000000002334
- Huang C, Irwin MG, Wong GTC, Chang RCC. Evidence of the impact of systemic inflammation on neuroinflammation from a non-bacterial endotoxin animal model. *J Neuroinflammation*. (2018) 15:147. doi: 10.1186/s12974-018-1163-z
- Ho YS, Cheng WY, Lai MSL, Lau CF, Wong GTC, Yeung WF, et al. Postoperative electroacupuncture boosts cognitive function recovery after laparotomy in mice. *Biomolecules*. (2024) 14:1274. doi: 10.3390/biom14101274
- Lu Y, Xu X, Dong R, Sun L, Chen L, Zhang Z, et al. MicroRNA-181b-5p attenuates early postoperative cognitive dysfunction by suppressing hippocampal neuroinflammation in mice. *Cytokine*. (2019) 120:41–53. doi: 10.1016/j.cyt.2019.04.005
- Xu J, Dong H, Qian Q, Zhang X, Wang Y, Jin W, et al. Astrocyte-derived CCL2 participates in surgery-induced cognitive dysfunction and neuroinflammation via evoking microglia activation. *Behav Brain Res*. (2017) 332:145–53. doi: 10.1016/j.bbr.2017.05.066
- Degos V, Vacas S, Han Z, van Rooijen N, Gressens P, Su H, et al. Depletion of bone marrow-derived macrophages perturbs the innate immune response to surgery

appreciate Mr. Justin Man Hin Wong's assistance in experiments, and staff from CCMR for animal experiments, and the Centre for PanorOmic Sciences for guidance on confocal imaging and flow cytometry.

Conflict of interest

The authors declare that the research was conducted in the absence of any commercial or financial relationships that could be construed as a potential conflict of interest.

The author(s) declared that they were an editorial board member of Frontiers, at the time of submission. This had no impact on the peer review process and the final decision.

Publisher's note

All claims expressed in this article are solely those of the authors and do not necessarily represent those of their affiliated organizations, or those of the publisher, the editors and the reviewers. Any product that may be evaluated in this article, or claim that may be made by its manufacturer, is not guaranteed or endorsed by the publisher.

Supplementary material

The Supplementary Material for this article can be found online at: <https://www.frontiersin.org/articles/10.3389/fimmu.2025.1469737/full#supplementary-material>

- and reduces postoperative memory dysfunction. *Anesthesiology*. (2013) 118:527–36. doi: 10.1097/ALN.0b013e3182834d94
17. Poon DCH, Ho YS, You R, Tse HL, Chiu K, Chang RCC. PKR deficiency alters E. coli-induced sickness behaviors but does not exacerbate neuroimmune responses or bacterial load. *J Neuroinflammation*. (2015) 12:212. doi: 10.1186/s12974-015-0433-2
18. Carret-Rebillat AS, Pace C, Gourmaud S, Ravasi L, Montagne-Stora S, Longueville S, et al. Neuroinflammation and A β accumulation linked to systemic inflammation are decreased by genetic PKR down-regulation. *Sci Rep*. (2015) 5:8489. doi: 10.1038/srep08489
19. Cheng WY, Chan PL, Ong HY, Wong KH, Chang RCC. Systemic inflammation disrupts circadian rhythms and diurnal neuroimmune dynamics. *Int J Mol Sci*. (2024) 25:7458. doi: 10.3390/ijms25137458
20. Seki S, Habu Y, Kawamura T, Takeda K, Dobashi H, Ohkawa T, et al. The liver as a crucial organ in the first line of host defense: the roles of Kupffer cells, natural killer (NK) cells and NK1.1 Ag+ T cells in T helper 1 immune responses. *Immunol Rev*. (2000) 174:35–46. doi: 10.1034/j.1600-0528.2002.017404.x
21. Garcia M, Meurs E, Esteban M. The dsRNA protein kinase PKR: virus and cell control. *Biochimie*. (2007) 89:799–811. doi: 10.1016/j.biochi.2007.03.001
22. Maggi LB, Heitmeier MR, Scheuner D, Kaufman RJ, Buller RML, Corbett JA. Potential role of PKR in double-stranded RNA-induced macrophage activation. *EMBO J*. (2000) 19:3630–8. doi: 10.1093/emboj/19.14.3630
23. Williams BRG. Signal integration via PKR. *Sci STKE*. (2001) 2001:re2–re. doi: 10.1126/stke.2001.89.re2
24. Goh KC, deVeer MJ, Williams BRG. The protein kinase PKR is required for p38 MAPK activation and the innate immune response to bacterial endotoxin. *EMBO J*. (2000) 19:4292–7. doi: 10.1093/emboj/19.16.4292
25. Zamanian-Daryoush M, Mogensen TH, DiDonato JA, Williams BRG. NF- κ B activation by double-stranded-RNA-activated protein kinase (PKR) is mediated through NF- κ B-inducing kinase and I κ B kinase. *Mol Cell Biol*. (2000) 20:1278. doi: 10.1128/MCB.20.4.1278-1290.2000
26. Yim HCH, Williams BRG. Protein kinase R and the inflammasome. *J Interferon Cytokine Res*. (2014) 34:447–54. doi: 10.1089/jir.2014.0008
27. Lu B, Nakamura T, Inouye K, Li J, Tang Y, Lundback P, et al. Novel role of PKR in inflammasome activation and HMGB1 release. *Nature*. (2012) 488:670–4. doi: 10.1038/nature11290
28. Chang RCC, Suen KC, Ma CH, Elyaman W, Ng HK, Hugon J. Involvement of double-stranded RNA-dependent protein kinase and phosphorylation of eukaryotic initiation factor-2 α in neuronal degeneration. *J Neurochem*. (2002) 83:1215–25. doi: 10.1046/j.1471-4159.2002.01237.x
29. Zhu Ping J, Huang W, Kalikulov D, Yoo Jong W, Placzek Andon N, Stoica L, et al. Suppression of PKR promotes network excitability and enhanced cognition by interferon- γ -mediated disinhibition. *Cell*. (2011) 147:1384–96. doi: 10.1016/j.cell.2011.11.029
30. Nakamura T, Kunz RC, Zhang C, Kimura T, Yuan CL, Baccaro B, et al. A critical role for PKR complexes with TRBP in Immunometabolic regulation and eIF2 α phosphorylation in obesity. *Cell Rep*. (2015) 11:295–307. doi: 10.1016/j.celrep.2015.03.021
31. Nakamura T, Arduini A, Baccaro B, Furuhashi M, Hotamisligil GS. Small-molecule inhibitors of PKR improve glucose homeostasis in obese diabetic mice. *Diabetes*. (2014) 63:526–34. doi: 10.2337/db13-1019
32. Gu C, Wang F, Zhang YT, Wei SZ, Liu JY, Sun HY, et al. Microglial MT1 activation inhibits LPS-induced neuroinflammation via regulation of metabolic reprogramming. *Aging Cell*. (2021) 20:e13375. doi: 10.1111/acel.13375
33. Baik SH, Kang S, Lee W, Choi H, Chung S, Kim J-I, et al. A breakdown in metabolic reprogramming causes microglia dysfunction in Alzheimer's disease. *Cell Metab*. (2019) 30:493–507.e6. doi: 10.1016/j.cmet.2019.06.005
34. Malkov A, Popova I, Ivanov A, Jang SS, Yoon SY, Osypov A, et al. A β initiates brain hypometabolism, network dysfunction and behavioral abnormalities via NOX2-induced oxidative stress in mice. *Commun Biol*. (2021) 4:1054. doi: 10.1038/s42003-021-02551-x
35. Firbank MJ, Yarnall AJ, Lawson RA, Duncan GW, Khoo TK, Petrides GS, et al. Cerebral glucose metabolism and cognition in newly diagnosed Parkinson's disease: ICICLE-PD study. *J Neurol Neurosurg Psychiatry*. (2017) 88:310. doi: 10.1136/jnnp-2016-313918
36. Nakamura T, Furuhashi M, Li P, Cao H, Tuncman G, Sonenberg N, et al. Double-stranded RNA-dependent protein kinase links pathogen sensing with stress and metabolic homeostasis. *Cell*. (2010) 140:338–48. doi: 10.1016/j.cell.2010.01.001
37. Carvalho-Filho MA, Carvalho BM, Oliveira AG, Guadagnini D, Ueno M, Dias MM, et al. Double-stranded RNA-activated protein kinase is a key modulator of insulin sensitivity in physiological conditions and in obesity in mice. *Endocrinology*. (2012) 153:5261–74. doi: 10.1210/en.2012-1400
38. Ouchi Y, Fukuyama H, Ogawa M, Yamauchi H, Kimura J, Magata Y, et al. Cholinergic projection from the basal forebrain and cerebral glucose metabolism in rats: A dynamic PET study. *J Cereb Blood Flow Metab*. (1996) 16:34–41. doi: 10.1097/00004647-199601000-00004
39. Rossi J, Balthasar N, Olson D, Scott M, Berglund E, Lee CE, et al. Melanocortin-4 receptors expressed by cholinergic neurons regulate energy balance and glucose homeostasis. *Cell Metab*. (2011) 13:195–204. doi: 10.1016/j.cmet.2011.01.010
40. You R, Liu Y, Chang RC. A behavioral test battery for the repeated assessment of motor skills, mood, and cognition in mice. *J Vis Exp*. (2019) 145. doi: 10.3791/58973
41. Ho YS, Lau CF, Lee K, Tan JY, Lee J, Yung S, et al. Impact of unilateral ureteral obstruction on cognition and neurodegeneration. *Brain Res Bull*. (2021) 169:112–27. doi: 10.1016/j.brainresbull.2021.01.001
42. Wang RPH, Huang J, Chan KKY, Leung WK, Goto T, Ho YS, et al. IL-1 β and TNF- α play an important role in modulating the risk of periodontitis and Alzheimer's disease. *J Neuroinflammation*. (2023) 20:71. doi: 10.1186/s12974-023-02747-4
43. O'Connor AM, Burton TJ, Leamey CA, Sawatari A. The use of the puzzle box as a means of assessing the efficacy of environmental enrichment. *J Vis Exp*. (2014) 94. doi: 10.3791/52225
44. Young K, Morrison H. Quantifying microglia morphology from photomicrographs of immunohistochemistry prepared tissue using ImageJ. *J Vis Exp*. (2018) 136:e57648. doi: 10.3791/57648
45. Bao J, Tan S, Yu W, Lin Z, Dong Y, Chen Q, et al. The effect of peritoneal air exposure on intestinal mucosal barrier. *Gastroenterol Res Pract*. (2014) 2014:674875. doi: 10.1155/2014/674875
46. Tan S, Yu W, Lin Z, Chen Q, Shi J, Dong Y, et al. Peritoneal air exposure elicits an intestinal inflammation resulting in postoperative ileus. *Mediators Inflamm*. (2014) 2014:924296. doi: 10.1155/2014/924296
47. Jacobi CA, Ordemann J, Zieren HU, Volk HD, Bauhofer A, Halle E, et al. Increased systemic inflammation after laparotomy vs laparoscopy in an animal model of peritonitis. *Arch Surg*. (1998) 133:258–62. doi: 10.1001/archsurg.133.3.258
48. Cheng WY, Ho YS, Chang RCC. Linking circadian rhythms to microbiome-gut-brain axis in aging-associated neurodegenerative diseases. *Ageing Res Rev*. (2022) 78:101620. doi: 10.1016/j.arr.2022.101620
49. Shaftel SS, Griffin WST, O'Banion MK. The role of interleukin-1 in neuroinflammation and Alzheimer disease: an evolving perspective. *J Neuroinflammation*. (2008) 5:7. doi: 10.1186/1742-2094-5-7
50. Saghazadeh A, Ferrari CC, Rezaei N. Deciphering variability in the role of interleukin-1 β in Parkinson's disease. *Rev Neurosci*. (2016) 27:635–50. doi: 10.1515/revneuro-2015-0059
51. Moynagh PN. The interleukin-1 signalling pathway in astrocytes: a key contributor to inflammation in the brain. *J Anat*. (2005) 207:265–9. doi: 10.1111/j.1469-7580.2005.00445.x
52. Takada Y, Ichikawa H, Pataer A, Swisher S, Aggarwal BB. Genetic deletion of PKR abrogates TNF-induced activation of IkappaBalpha kinase, JNK, Akt and cell proliferation but potentiates p44/p42 MAPK and p38 MAPK activation. *Oncogene*. (2007) 26:1201–12. doi: 10.1038/sj.onc.1209906
53. Couturier J, Paccalin M, Morel M, Terro F, Milin S, Pontcharraud R, et al. Prevention of the β -amyloid peptide-induced inflammatory process by inhibition of double-stranded RNA-dependent protein kinase in primary murine mixed co-cultures. *J Neuroinflammation*. (2011) 8:72. doi: 10.1186/1742-2094-8-72
54. He Y, Franchi L, Núñez G. The protein kinase PKR is critical for LPS-induced iNOS production but dispensable for inflammasome activation in macrophages. *Eur J Immunol*. (2013) 43:1147–52. doi: 10.1002/eji.201243187
55. McNeill E, Crabtree MJ, Sahgal N, Patel J, Chuaiphichai S, Iqbal AJ, et al. Regulation of iNOS function and cellular redox state by macrophage Gch1 reveals specific requirements for tetrahydrobiopterin in NRF2 activation. *Free Radic Biol Med*. (2015) 79:206–16. doi: 10.1016/j.freeradbiomed.2014.10.575
56. Rosas-Ballina M, Tracey KJ. Cholinergic control of inflammation. *J Intern Med*. (2009) 265:663–79. doi: 10.1111/j.1365-2796.2009.02098.x
57. Stern E, Chinnakkaruppan A, David O, Sonenberg N, Rosenblum K. Blocking the eIF2 α Kinase (PKR) enhances positive and negative forms of cortex-dependent taste memory. *J Neurosci*. (2013) 33:2517. doi: 10.1523/JNEUROSCI.2322-12.2013
58. Jiang Z, Belforte JE, Lu Y, Yabe Y, Pickel J, Smith CB, et al. eIF2 α phosphorylation-dependent translation in CA1 pyramidal cells impairs hippocampal memory consolidation without affecting general translation. *J Neurosci*. (2010) 30:2582. doi: 10.1523/JNEUROSCI.3971-09.2010
59. Drzezga A, Lautenschlager N, Siebner H, Riemenschneider M, Willoch F, Minoshima S, et al. Cerebral metabolic changes accompanying conversion of mild cognitive impairment into Alzheimer's disease: a PET follow-up study. *Eur J Nucl Med Mol Imaging*. (2003) 30:1104–13. doi: 10.1007/s00259-003-1194-1
60. Mosconi L, Pupi A, De Leon MJ. Brain glucose hypometabolism and oxidative stress in preclinical Alzheimer's disease. *Ann N Y Acad Sci*. (2008) 1147:180–95. doi: 10.1196/annals.1427.007
61. Bergau N, Maul S, Rujescu D, Simm A, Navarrete Santos A. Reduction of glycolysis intermediate concentrations in the cerebrospinal fluid of Alzheimer's disease patients. *Front Neurosci*. (2019) 13:871. doi: 10.3389/fnins.2019.00871
62. Stovell MG, Mada MO, Helmy A, Carpenter TA, Thelin EP, Yan J-L, et al. The effect of succinate on brain NADH/NAD $^{+}$ redox state and high energy phosphate metabolism in acute traumatic brain injury. *Sci Rep*. (2018) 8:11140. doi: 10.1038/s41598-018-29255-3
63. Khellaf A, Garcia NM, Tajsic T, Alam A, Stovell MG, Killen MJ, et al. Focally administered succinate improves cerebral metabolism in traumatic brain injury patients with mitochondrial dysfunction. *J Cereb Blood Flow Metab*. (2022) 42:39–55. doi: 10.1177/0271678x211042112
64. Carvalho BM, Oliveira AG, Ueno M, Aratijo TG, Guadagnini D, Carvalho-Filho MA, et al. Modulation of double-stranded RNA-activated protein kinase in insulin sensitive tissues of obese humans. *Obes (Silver Spring)*. (2013) 21:2452–7. doi: 10.1002/oby.20410